The first complete 3D reconstruction and morphofunctional mapping of an insect eye

Anastasia A. Makarova[1], Nicholas J. Chua[2], Anna V. Diakova[1], Inna A. Desyatirkina[1], Pat Gunn[2], Song Pang [3,4], C. Shan Xu [3,5], Harald Hess[3], Dmitri B. Chklovskii[2,6], Alexey A. Polilov*[1]

[1]Department of Entomology, Faculty of Biology, Lomonosov Moscow State University, Moscow, Russia.
[2]Center for Computational Neuroscience, Flatiron Institute, New York, NY, USA
[3]Janelia Research Campus, Howard Hughes Medical Institute, Ashburn, USA.
[4]Yale School of Medicine, New Haven, CT, USA.
[5]Department of Cellular and Molecular Physiology, Yale School of Medicine, New Haven, CT, USA.
[6]Neuroscience Institute, NYU Langone Medical Center, New York, NY, USA.
*email: polilov@gmail.com

Abstract

The structure of compound eyes in arthropods has been the subject of many studies revealing important biological principles. However, until recently, these studies were constrained by the two-dimensional nature of available ultrastructural data. Here, by taking advantage of the novel three-dimensional ultrastructural dataset obtained using volume electron microscopy (vEM), we present the first cellular-level reconstruction of the whole compound eye of an insect, the extremely miniaturized parasitoid wasp *Megaphragma viggianii*. The compound eye of the female *M. viggianii* consists of 29 ommatidia and contains 478 cells. Despite the almost anucleate brain, all cells of the compound eye possess nuclei. Like in larger insects, the dorsal rim area (DRA) of the *M. viggianii* eye contains ommatidia that putatively specialize in the polarized light detection as reflected in their corneal and retinal morphology. We report the presence of three 'ectopic' photoreceptors. Our results offer new insights into the miniaturization of compound eyes and scaling of sensory organs in general.

1. Introduction

Sensory organs are essential for informing the animal about its environment and, hence, for survival. Their study has revealed important biological principles even in simpler organisms such as insects (Borst, Egelhaaf, 1989; Strausfeld, 1989; Warrant, McIntyre, 1993; Meyer-Rochow, 2015; Meyer-Rochow, Gal, 2004; Warrant, Nilsson, 2006; Borst, 2009). The study of the principles of the scaling in sensory organs is a highly interesting and complex objective for morphology and bionics (Srinivasan et al., 1999; Graham, Philippides, 2012; Serres, Viollet, 2018). Most ultrastructural studies on insect sensory organs are currently performed using traditional scanning EM (external morphology) and/or single-section transmission EM (internal ultrastructure). Because these methods scan only parts of the sensory organs they were not giving us the full picture. The modern methods of volume electron microscopy (vEM) give us great opportunities for studying the structure of insects at the ultrastructural level (Meinertzhagen, 2018, Kawasaki et al., 2019). However, the peculiar constructive features of these methods often limit the minimum size of the studied organisms (Xu et al., 2017). The methods of vEM require complex material staining, much time for scanning, and a disproportionally long period for proofreading (Plaza et al., 2014), and as a result reconstructions of whole organisms (whole-body connectomics) using vEM are rather scarce and

deal with very simple animals (White, 1986; Varshney et al. 2011; Ryan et al., 2016; Cook et al., 2019; Jékely et al., 2024).

Minute insects are convenient and extremely interesting organisms for study, because they have many physiological, cognitive, and behavioral capacities found in larger insects and, at the same time, their extremely small body sizes make it possible to reconstruct in detail not only their sensory organs (Diakova et al., 2021), but also whole organ systems (Desyatirkina et al., 2023), and to trace the complete pathways that connect their sense organs with particular regions of the brain (Chua et al., 2023). Three-dimensional (3D) reconstructions of sensory organs make it possible to assess and test the data obtained earlier using traditional electron microscopy, specify the spatial orientation, shape, and volumetric parameters of cells and organelles. Three ommatidia of a compound eye were reconstructed in 3D for the first time in the parasitoid wasp *Trichogramma evanescens* (Fischer et al., 2019), a study that considerably broadened our notions of the functional and structural limits in miniaturized sense organs. In spite of the progress in methods of electron microscopy, until now a detailed 3D description of a complete compound eye has never been published.

The peculiar features of structure and function of compound eyes, ultrastructure of photoreceptors, and the associated functional and structural limits of insects associated with small body sizes were studied in detail in several insect orders: Coleoptera (Meyer-Rochow, Gal, 2004; Makarova, Polilov, 2018; Makarova et al., 2019), Hymenoptera (Fischer et al., 2011; Makarova et al., 2015; Palavalli-Nettimi, Narendra, 2018; Fischer et al., 2019; Palavalli-Nettimi et al., 2019), Diptera (Meyer-Rochow, Yamahama, 2019), and Lepidoptera (Honkanen, Meyer-Rochow, 2009; Fischer et al., 2011a, 2012, 2014); for review, see Makarova et al. (2022, 2022a). In spite of the considerable progress in the study of the miniaturization of compound eyes, some issues have remained incompletely investigated (e.g., the structure and spatial position of cells and subcellular elements of the eye or the functional specialization of ommatidia).

Megaphragma viggianii is a minute parasitic wasps, one of the smallest known species of the family Trichogrammatidae, an egg parasite of thrips (Bernardo, Viggiani, 2002). Three species of *Megaphragma* are known to display the phenomenon of the lysis of nuclei in neurons during the later periods of pupal development (Polilov, 2012; 2017; Makarova et al., 2022). The general structural organization of compound eyes and adaptations associated with miniaturization were described on the basis of single EM sections in *M. polilovi* (Makarova et al., 2015). Data on the optical properties of the ommatidia and the connectome of the first visual neuropil (the lamina) were first obtained using the full dataset of a *Megaphragma* head (Chua et al., 2023).

The main goal of this study is to reveal the ultrastructural organization of compound eyes in the extremely small insect *M. viggianii*. Complete cellular reconstruction of compound eyes using vEM based on focused ion beam (FIB) SEM makes it possible not only to visualize the 3D structure of the whole eye but also to trace the pathways that connect the analyzer with the brain. Morphometric analysis, in turn, makes it possible to specify the number and cellular composition of ommatidia and assess the sizes and volumes of subcellular elements, providing novel and unique data on the scaling of sense organs.

2. Results

2.1. General description of the compound eye

The female compound eyes of the parasitoid wasp *M. viggianii* are oval in shape (Figure 1A) and measure about 50.6 ± 1.5 µm (hereinafter mean ± s.d.) in dorso-ventral extent. Their anterior-posterior extent is on average 32.6 ± 0.73 µm. Each eye has 29 facets. The corneal surface of the facets is smooth. A single interfacet bristle is present near the posterior row of the eye, between facets E5, D5, D4 (Figure 1B). No differences are visible on SEM (at the external cuticular level) between the facets of the eye.

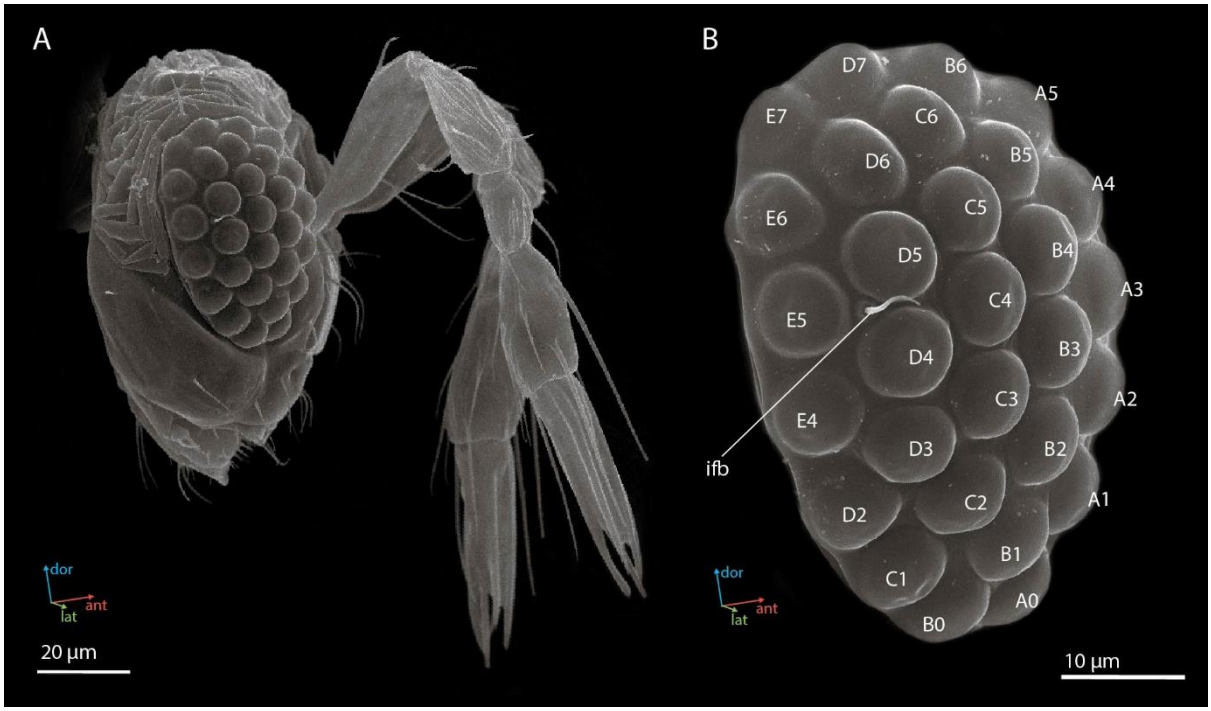

Figure 1. Scanning electron microscopy (SEM) images of the head (A) and the compound eye (B) of a female *Megaphragma viggianii* (side view). Ifb – inter-facet bristle. The compound eye comprises 29 ommatidia named as in Chua et al. (2023).

2.2. General description of ommatidia

Using the vEM of the whole *M. viggianii* eye we found that it contains a total of 478 cells: 261 photoreceptor cells, 116 cone cells, 58 primary pigment cells, 24 secondary pigment cells, 16 rim pigment cells (surrounding the eye on the periphery), and 3 ectopic photoreceptors (see below, 2.2.5. *'Ectopic' photoreceptors*). Each of the 29 ommatidia contains nine photoreceptor cells, four cone cells, and two primary pigment cells (Figure 2A). The length of one ommatidium is on average 21.2 µm, gradually increasing from the dorsal rim area (DRA) to the ventral part of the eye (Table 1).

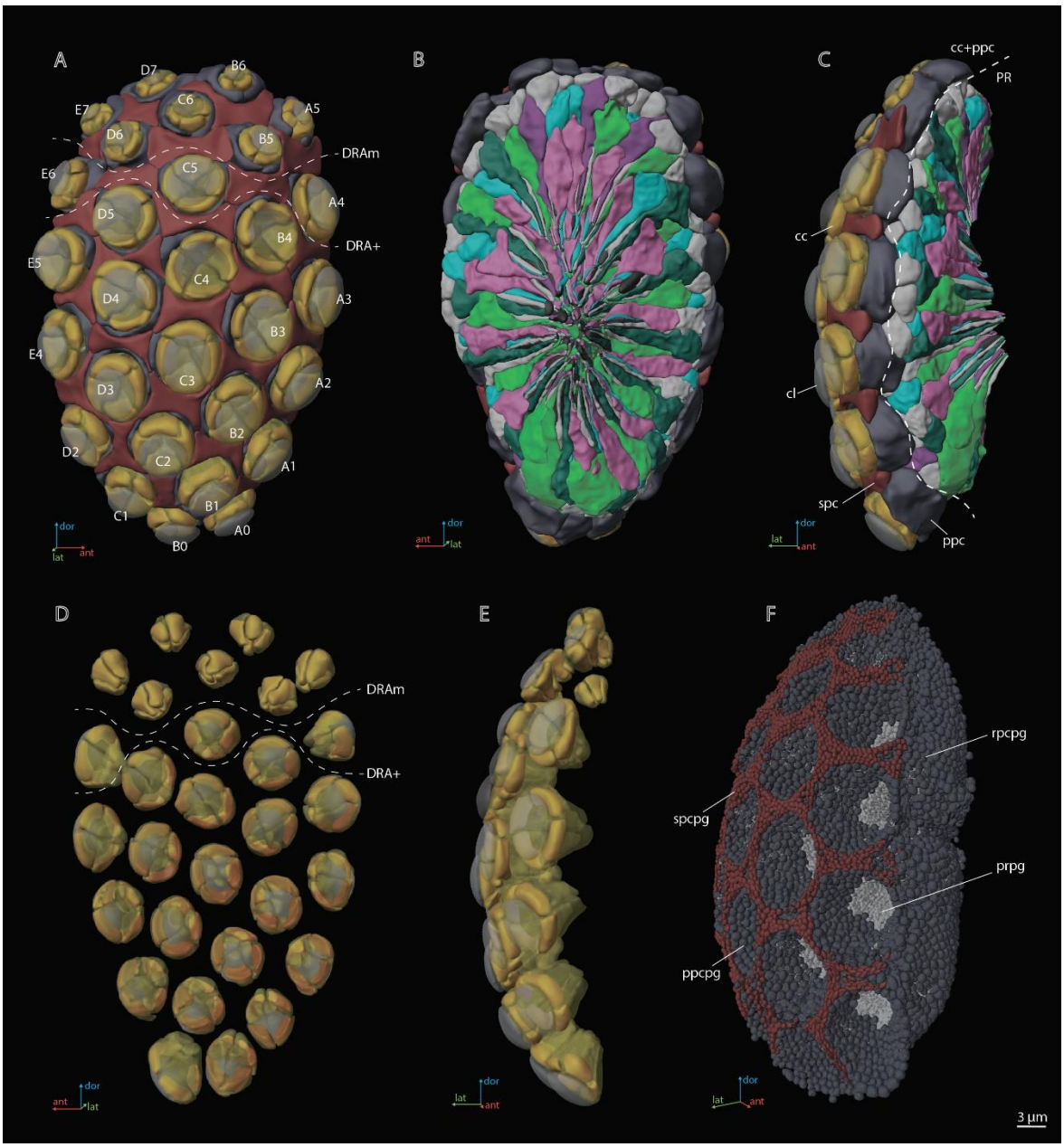

Figure 2. A three-dimensional (3D) reconstruction of a compound eye of *M. viggianii*. A. A front view from the cornea side; B. A rear view from the retinal side; C. A side view; D. A rear view of the ommatidia DA; E. A rear view of the ommatidia DA; F. A semi-side view of pigment granules of all cells. Abbreviations: cc – crystalline cones; cl – corneal lense; DRAm – dorsal rim area ommatidia (morphological specialization); DRA+ – transitional zone ommatidia; ppc – primary pigment cells; ppcpg – pigment granules of PPC; prpg – retinal (photoreceptor) pigment granules; rpcpg – rim cells pigment granules; spc – secondary pigment cells; spcpg – secondary pigment cell pigment granules. Ommatidia are named as in Chua et al. (2023).

Table 1. Linear measurements (µm) of *M. viggianii* eye components. Diameter[1,2] – diameter of rhabdom measured in orthogonal planes, according to its not round shape. Hereinafter mean ± s.d. DRA – dorsal rim ommatidia in general (DRAm and DRA+); DRAm – dorsal rim area ommatidia (morphological specialization); DRA+ – transitional zone ommatidia; Non-DRA – regular ommatidia. Raw data—Table S1.

	Ommatidium length	Lense				Cone		Rhabdom				
		Diameter	Thikness	Curvature		Length	Wigth	Diameter (distal)	Diameter central[1]	Diameter central[2]	Diameter mean	Length
				inner	outer							
DRA	19.2 ± 0.37	6.9 ± 0.89	2.5 ± 0.56	1.2 ± 0.32	3.3 ± 0.64	3.0 ± 0.38	4.9 ± 0.66	2.0 ± 0.16	2.1 ± 0.32	2.2 ± 0.23	2.1 ± 0.18	13.4 ± 0.64
DRAm	19.0 ± 0.20	6.5 ± 0.51	2.2 ± 0.28	1.1 ± 0.21	3.1 ± 0.51	2.8 ± 0.28	4.5 ± 0.21	1.9 ± 0.11	1.9 ± 0.16	2.2 ± 0.24	2.1 ± 0.11	13.7 ± 0.29
DRA+	19.7 ± 0.15	7.9 ± 0.85	3.2 ± 0.26	1.6 ± 0.19	3.9 ± 0.68	3.4 ± 0.14	5.8 ± 0.21	2.2 ± 0.068	2.5 ± 0.21	2.2 ± 0.25	2.4 ± 0.11	12.6 ± 0.63
non-DRA	22.3 ± 2.5	8.0 ± 0.77	3.3 ± 0.40	3.0 ± 0.52	4.7 ± 0.39	4.6 ± 0.60	6.7 ± 0.25	2.7 ± 0.26	2.9 ± 0.25	2.8 ± 0.27	2.9 ± 0.21	14.2 ± 1.8

Table 2. Mean volumes (µm^3) for cellular and subcellular elements of ommatidia in *M. viggianii*. The volumes were obtained from 3D models. DRA – dorsal rim ommatidia in general (DRAm and DRA+); DRAm – dorsal rim area ommatidia (morphological specialization); DRA+ – transitional zone ommatidia; Non-DRA – regular (non-DRA) ommatidia; R1-R8 – retinal cells; PPC – primary pigment cells; SPC – secondary pigmen cells. Raw data—Table S2.

		Retinal cell									Cone	PPC	SPC	Lense
		R1	R2	R3	R7'	R4	R5	R6	R7	R8				
Soma	DRA	17.5 ± 2.0	24.4 ± 3.8	17.9 ± 2.3	33.0 ± 2.5	18.0 ± 2.0	25.2 ± 4.1	17.9 ± 1.6	32.1 ± 4.8	15.8 ± 1.9	13.1 ± 6.0	47.1 ± 14.4	22.0 ± 4.7	16.5 ± 14.0
	DRAm	16.4 ± 1.2	22.3 ± 2.3	17.7 ± 2.3	32.2 ± 2.0	17.2 ± 1.4	23.4 ± 3.1	17.1 ± 0.8	30.0 ± 3.4	14.8 ± 0.8	9.5 ± 1.2	40.6 ± 9.5	20.2 ± 4.3	8.6 ± 3.3
	DRA+	19.8 ± 2.7	29.2 ± 3.7	18.3 ± 3.1	34.8 ± 3.7	20.0 ± 3.0	29.4 ± 4.3	19.9 ± 1.9	37.2 ± 6.7	18.2 ± 2.5	21.3 ± 4.5	61.4 ± 13.0	26.2 ± 2.6	34.8 ± 17.2
	non-DRA	21.0 ± 3.3	29.5 ± 3.1	22.0 ± 2.6	53.3 ± 11.1	22.4 ± 3.5	31.1 ± 3.2	20.5 ± 4.5	30.6 ± 8.5	28.2 ± 4.3	32.9 ± 5.9	64.5 ± 11.4	24.5 ± 3.2	41.4 ± 9.0
Nuclei	DRA	6.5 ± 0.46	7.2 ± 0.89	6.7 ± 0.64	8.2 ± 0.83	6.7 ± 0.52	7.4 ± 0.73	6.8 ± 0.36	8.4 ± 1.03	7.0 ± 0.63	6.6 ± 0.59	7.5 ± 0.86	6.6 ± 0.78	n/a
	DRAm	6.4 ± 0.42	6.8 ± 0.72	6.8 ± 0.62	8.4 ± 0.61	6.7 ± 0.53	7.3 ± 0.66	6.8 ± 0.38	8.3 ± 0.98	6.8 ± 0.53	6.5 ± 0.65	7.4 ± 0.93	6.8 ± 0.76	n/a
	DRA+	6.8 ± 0.73	8.0 ± 1.2	6.4 ± 0.75	7.6 ± 1.1	6.8 ± 0.60	7.7 ± 0.72	6.9 ± 0.47	8.6 ± 0.87	7.4 ± 0.73	6.9 ± 0.38	7.5 ± 0.75	5.9 ± 0.42	n/a
	non-DRA	7.0 ± 0.56	7.6 ± 0.91	7.2 ± 0.73	9.2 ± 1.1	7.2 ± 0.85	7.9 ± 0.71	6.9 ± 0.98	7.9 ± 1.2	8.3 ± 0.80	7.5 ± 0.93	7.6 ± 0.98	6.4 ± 1.0	n/a
Rhabdomere	DRA	1.8 ± 0.55	3.1 ± 0.74	2.3 ± 0.58	3.9 ± 0.81	1.7 ± 0.27	3.2 ± 0.69	1.8 ± 0.83	4.2 ± 1.1	0.86 ± 0.25	n/a	n/a	n/a	n/a
	DRAm	1.5 ± 0.28	2.7 ± 0.46	2.0 ± 0.44	3.5 ± 0.4	1.7 ± 0.26	2.9 ± 0.34	1.4 ± 0.59	3.6 ± 0.47	0.73 ± 0.05	n/a	n/a	n/a	n/a
	DRA+	2.4 ± 0.19	4.0 ± 0.46	2.9 ± 0.58	4.8 ± 0.61	1.9 ± 0.21	4.1 ± 0.53	2.6 ± 0.39	5.7 ± 1.6	1.2 ± 0.42	n/a	n/a	n/a	n/a
	non-DRA	4.1 ± 1.6	5.6 ± 1.3	3.2 ± 0.9	12.7 ± 3.9	3.6 ± 1.3	5.9 ± 1.0	3.2 ± 0.74	5.5 ± 2.1	6.7 ± 1.6	n/a	n/a	n/a	n/a

2.2.1. The dioptric apparatus

The dioptric apparatus (DA) of each ommatidium consists of the biconvex lens and crystalline cone (Figs. 2D, E; 3A, G). The diameter of the lens is 6.9 ± 0.89 µm in DRA and 8.0 ± 0.77 µm in non-DRA ommatidia (Table 1). The lenses are covered by cuticle of 0.28 ± 0.050 µm depth (Figure 3A, G). The greatest thickness of the lens is 2.5 ± 0.56 µm in DRA and 3.3 ± 0.40 µm in non-DRA ommatidia. The outer/inner radii of lens curvature are 3.3 ± 0.64 /1.2 ± 0.32 µm and 4.7 ± 0.39/ 3.0 ± 0.52 µm in DRA and non-DRA ommatidia, respectively. The volume of the lens is 16.5 ± 14.0 μm^3 in DRA and 41.4 ± 9.0 μm^3 in non-DRA (Table 2; Suppl. Table 2).

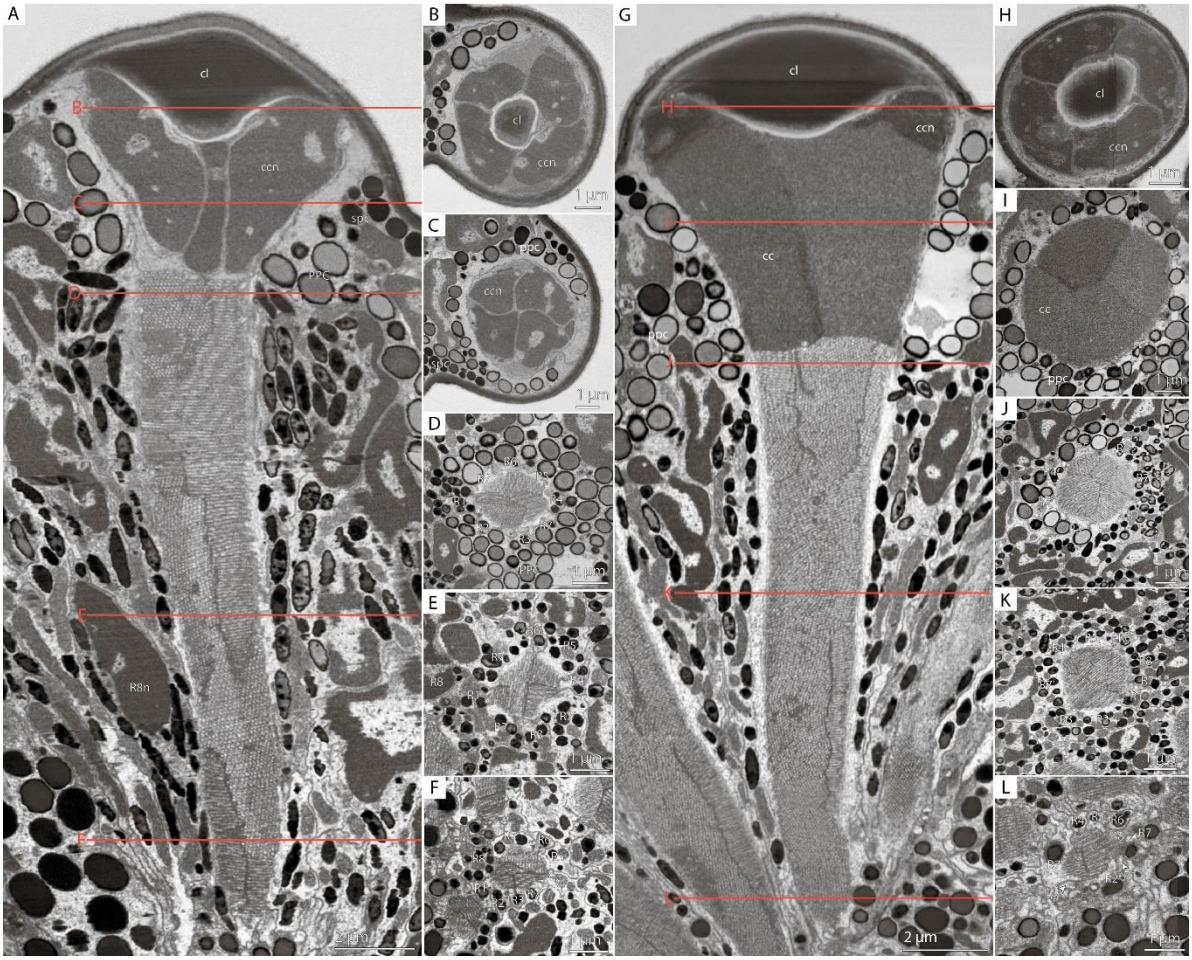

Figure 3. Cross-sections of *M. viggianii* ommatidia sampled from a vEM (FIB-SEM) dataset. A–F. DRA ommatidia (B5); G–L. non-DRA ommatidia (C3). A, G. A longitudinal section through one ommatidium; B, H. A cross-section through the proximal part of a corneal lens; C, I. A cross-section through the center of a cone; D, J. A cross-section through a distal rhabdom, directly under the cone; E, K. A cross-section through the center of a rhabdom; F, L. A cross-section through a distal rhabdom. Abbreviations: cc – crystalline cone; ccn – nuclei of crystalline cone cells; cl – corneal lens; ppc – primary pigment cells; R1–R8 – retinal cells; spc – secondary pigment cells; asterisk (*) marks cone cell projections.

The crystalline cone comprises four cone cells (Figure 2D, E; 3B, C, H, I; 4A, C). Each cone cell has a long and thin projection that extends down to the basal matrix along retinal cells (Figure 3 D–F, J – L). Due to the constant position of cone cell projections, we enumerate them according to their passing between the retinula cells: C1: between R1 and R1; C2: between R3 and R7'; C3: between

R4 and R5; C4: between R6 and R7(R8) (see *2.2.4. Retinula cells and rhabdom*) (Figure 3D–F; J, K). DRA ommatidia have small cones with nuclei that fill most of the cone cell volume (Figure 2D, E 3A–C; 4A, B, E, F, I, J). In DRA ommatidia the mean volume of a cone cell is 13.1 ± 6.0 μm^3 and of its nucleus: 6.6 ± 0.59 μm^3 (Table 2). In Non-DRA ommatidia the nuclei are elongated, positioned in the upper third of the cells perpendicular to the ommatidial long axis, leaving the central part of the cone free (Figs. 2D, E; 3 G, H, I; 4C, D, G, H, K, L; 5G, H, I). Reconstruction has shown that the nuclei of Non-DRA ommatidia form an aperture (Figure 2D; 4D, H). The mean volume of a cone cell in Non-DRA ommatidia is 32.9 ± 5.9 μm^3 and of its nucleus: 7.5 ± 0.93 μm^3 (Table 2).

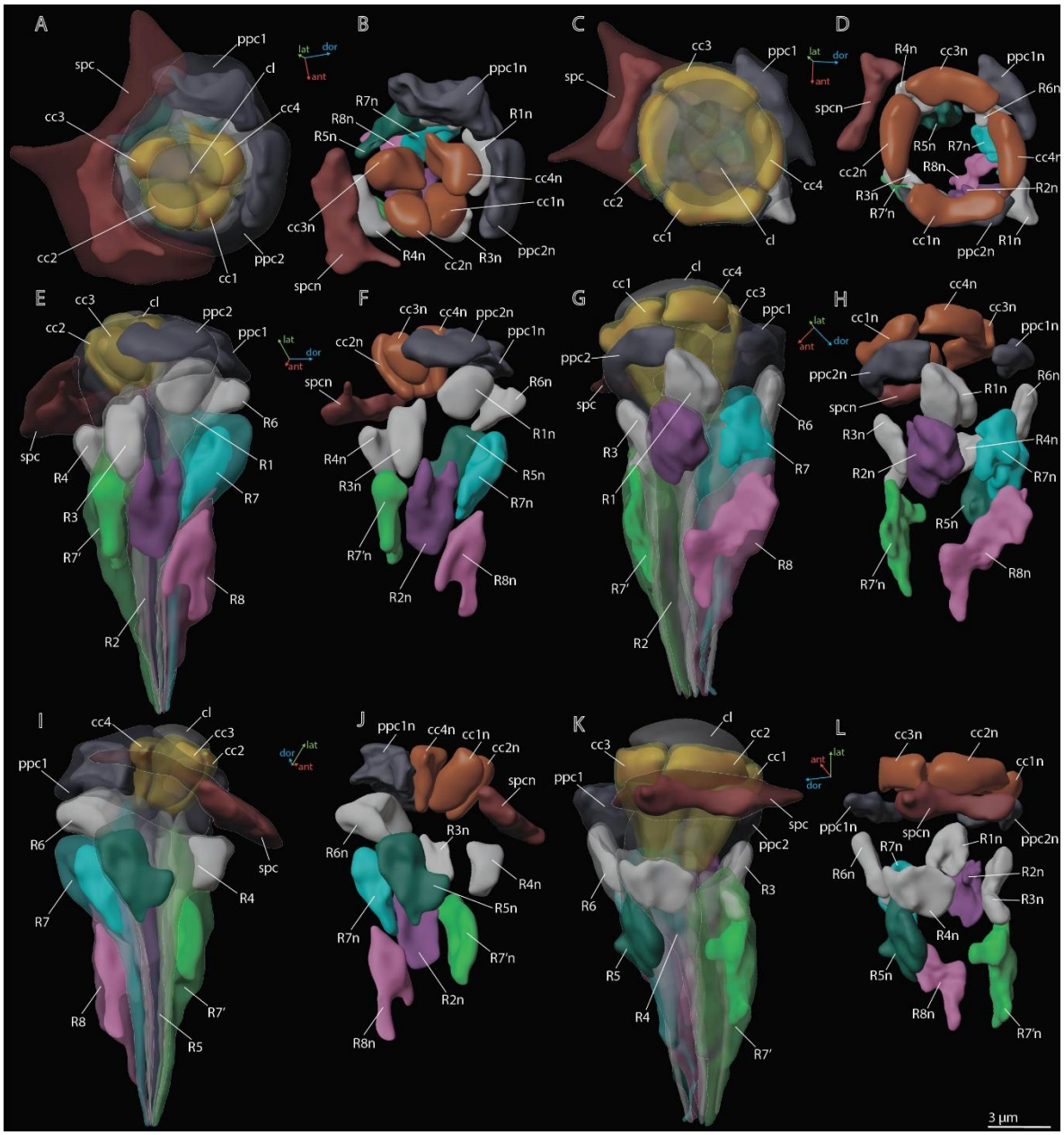

Figure 4. 3D reconstruction of nuclei in ommatidium cells of *M. viggianii*. A, B, E, F, I, J. DRA ommatidia (B6); C, D, G, H, K, L. Non-DRA ommatidia (C4). Abbreviations: cc1–4 – crystalline cone cells; cc1n–4n – nuclei of crystalline cone cells; cl – corneal lens; ppc1, 2 – primary pigment cells; ppc1n, ppc2n – nuclei of PPC; R1–R8 – retinal cells; R1n–8n – nuclei of retinal cells; spc – secondary pigment cells; spcn – nuclei of secondary pigment cells. Colors of nuclei same as colors of their cells.

2.2.2 Primary pigment cells (PPC)

Two primary pigment cells (PPC) envelope the cone of each ommatidium (Figure 2C, 3, 4) and are situated lower than the secondary pigment cells. The volume of PPC is 47.1 ± 14.4 μm^3 in DRA ommatidia and 64.5 ± 11.4 μm^3 in Non-DRA ommatidia (Table 2). The PPCs are densely filled with spherical pigment granules, identical in DRA and Non-DRA ommatidia (Figure 2F, 3, 5). The granules have a mean volume of 0.18 ± 0.039 μm^3. The PPC contain on average 144 ± 52 pigment granules, their total volume per cell being 26.9 ± 4.8 μm^3 (Table 3). The nuclei are positioned in the lower half of the cells, beneath the level of the secondary pigment cells (Figure 4). The volume of PPC nuclei is equal in DRA and Non-DRA ommatidia, their mean volume is 7.5 ± 0.94 μm^3 (7.5 ± 0.86 μm^3 and 7.6 ± 0.98 μm^3 for DRA and Non-DRA, respectively) (Table 2). Several small oval mitochondria are positioned in the dorsal half of PPC (Figure 6). The mean chondriome volume is 0.46 ± 0.14 μm^3.

Table 3. Volumes (μm^3) of pigment granules and mitochondria in ommatidia of *M. viggianii* and *Trichogramma evanescens*. The data for *T. evanescens* are from Fischer et al. (2019). R1–R8 – retinal cells; mt – mitochondria; pg – pigment granules; PPC – primary pigment cells; SPC – secondary pigmen cells. B6, C4, A3, A0 – ommatidia on which cells pigment granules and mitochondria were reconstructed. as – pigment granules were automatically segmented. Raw data—Table S2.

		Organelle type	R1	R2	R3	R7'	R4	R5	R6	R7	R8	PPC	SPC
M. viggianii	B6, D7, C4, A3, A0	PG	2.5 ± 0.71	3.2 ± 0.86	2.1 ± 0.51	6.5 ± 2.1	2.4 ± 0.31	2.7 ± 0.76	2.2 ± 0.36	5.5 ± 2.3	2.0 ± 1.0	26.98 ± 4.85	7.9 ± 3.0
		Mt	1.2 ± 0.40	1.8 ± 0.56	1.0 ± 0.32	2.8 ± 0.12	1.2 ± 0.39	1.8 ± 0.54	1.0 ± 0.42	2.0 ± 0.59	1.5 ± 0.96	0.53 ± 0.35	0.31 ± 0.070
T. evanescens	Three central ommatidia	PG	2.0 ± 0.12	2.1 ± 0.16	1.9 ± 0.07	2.5 ± 0.19	2.0 ± 0.14	2.1 ± 0.07	1.9 ± 0.15	3.0 ± 0.23	0.66 ± 0.12	8.5 ± 1.4	4.0 ± 0.53
		Mt	1.8 ± 0.08	2.8 ± 0.19	1.9 ± 0.05	1.4 ± 0.23	2.1 ± 0.08	2.8 ± 0.14	1.9 ± 0.14	1.8 ± 0.29	0.59 ± 0.05	0.46 ± 0.14	0.32 ± 0.09
M. viggianii	%	PG	12.1 ± 1.9	11.4 ± 1.8	11.2 ± 2.6	13.2 ± 1.7	10.5 ± 1.9	10.5 ± 1.5	10.3 ± 1.5	13.2 ± 1.7	8.9 ± 3.4	32.1 ± 11.5	26.1 ± 10.9
		Mt	5.7± 1.0	7.0 ± 1.8	4.9 ± 1.3	6.6 ± 1.8	5.5 ± 1.5	6.8 ± 1.0	5.0 ± 1.0	5.2 ± 0.51	5.0 ± 1.9	0.60 ± 0.0042	1.1 ± 0.42
T. evanescens		PG	11.3 ± 1.7	7.9 ± 0.63	9.6 ± 0.84	13.3 ± 2.1	11.4 ± 1.7	7.9 ± 0.81	11.2 ± 0.45	11.6 ± 0.43	7.8 ± 0.76	21.0 ± 0.94	19.1 ± 2.4
		Mt	9.8 ± 1.1	10.3 ± 0.72	9.5 ± 0.86	7.6 ± 0.51	11.6 ± 0.82	10.5 ± 0.27	11.0 ± 0.24	6.9 ± 0.75	6.9 ± 0.45	1.1 ± 0.17	1.5 ± 0.31

2.2.3. Secondary pigment cells (SPC)

24 secondary pigment cells (SPC) are positioned directly beneath the cornea (Figs. 2, 3, 4). Each ommatidium of the central part of the eye is surrounded by four SPCs, while each marginal ommatidium is surrounded only by two, on the internal margin of the eye (Figure 2A). No extensions of SPC adjoin the retinula cells down to the basal matrix. The volume of SPC is similar near DRA and Non-DRA ommatidia (Table 2). The nuclei of SPC have a mean volume of 6.4 ± 1.0 μm^3. The SPCs are filled with pigment granules (Figs. 2F, 5B, D), 158 ± 28 per cell, having a mean unit volume 0.050 ± 0.016 μm^3. The total volume of pigment granules per cell is about 7.9 ± 3.0 μm^3 (Table 3). The shape of the granules of SPC in the dorsal third of the eye, near the DRA ommatidia, is round. The shape of pigment granules in the center and proximal third of the eye (around the Non-DRA ommatidia) is oval (Figure 5B, D). Several small oval mitochondria are positioned in the dorsal half of SPC (Figure 6). The mean volume of the chondriome is 0.24 ± 0.15 μm^3.

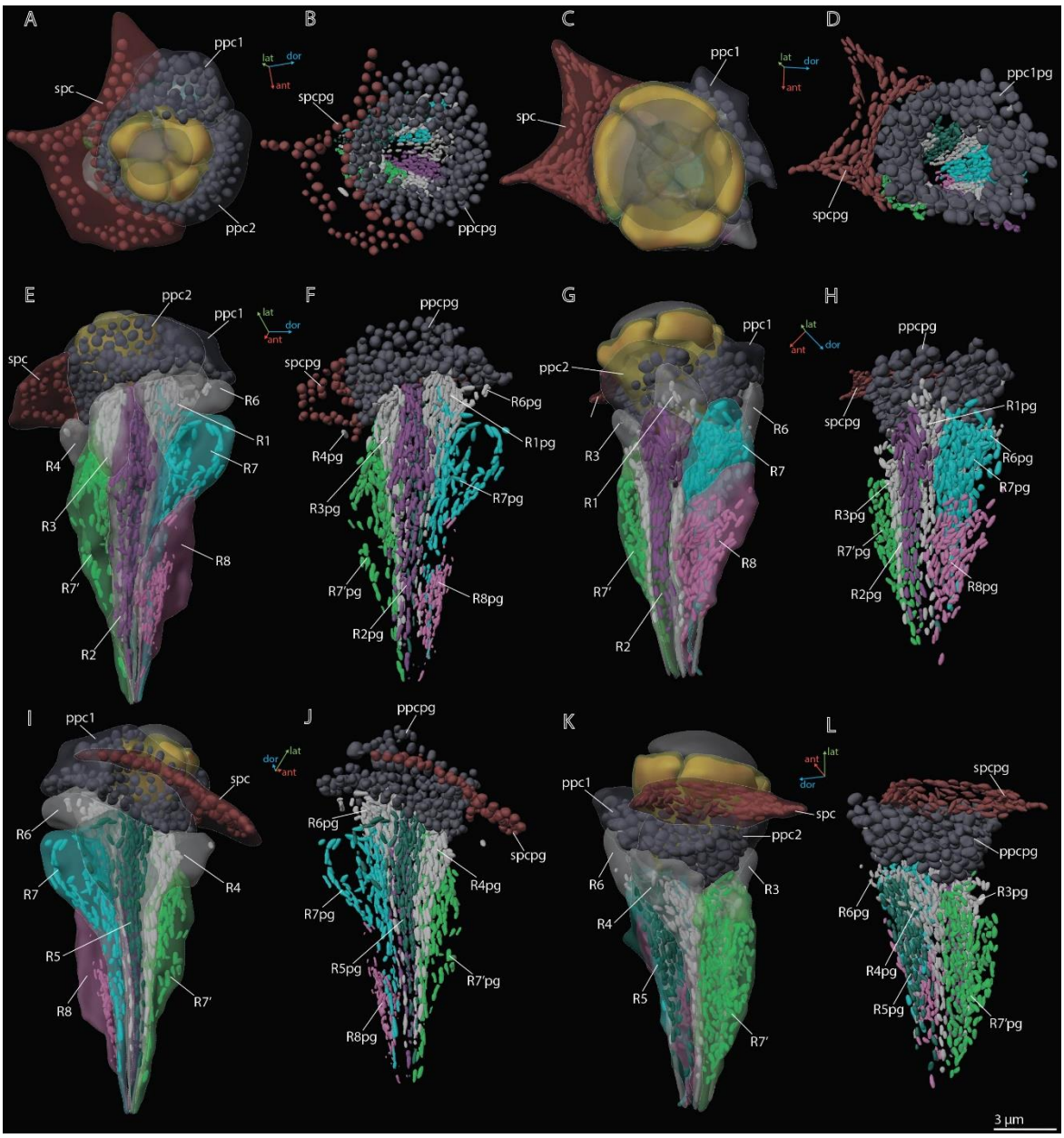

Figure 5. 3D reconstruction of pigment granules in the ommatidium cells of *M. viggianii*. A, B, E, F, I, J. DRA ommatidia (B6); C, D, G, H, K, L. Non-DRA ommatidia (C4). Abbreviations: ppc1, 2 – primary pigment cells; ppc1pg, ppc2pg – pigment granules of PPC; R1–R8 – retinal cells; R1pg–8pg – pigment granules of retinal cells; spc – secondary pigment cells; spcpg – pigment granules of secondary pigment cells. Colors of pigment granules same as colors of their cells.

2.2.4. Retinula cells and the rhabdom

The retina area of each ommatidium consists of nine photoreceptor cells (PR) (Figs. 3, 4; Suppl. 1 C), six of which (R1–R6) send short axons that project to the lamina and the remaining three (R7, R7', R8) - long axons that reach the medulla. The position of the eighth retinula cell in relation to the position of the cone cell projections and the axon targets in the optic lobes can be used for recognition and labelling of all other cells (see *Methods: Identifying the retinula cells and terminology*). The nuclei of retinula cells are arranged on four levels (Figure 4). The most distal position is occupied by the nuclei of PR R1, R3, R4, and R6. More proximally the nuclei of partner cells R2 and R5 are situated opposite each other and R7 PR. The nuclei of R7' and R8 PR are

positioned proximally; R8 is the lowest (Figure 4). The majority of R7 cells show lighter rhabdomeres (less electron density) than other PR (Figure 3D, J) (Suppl. 1C).

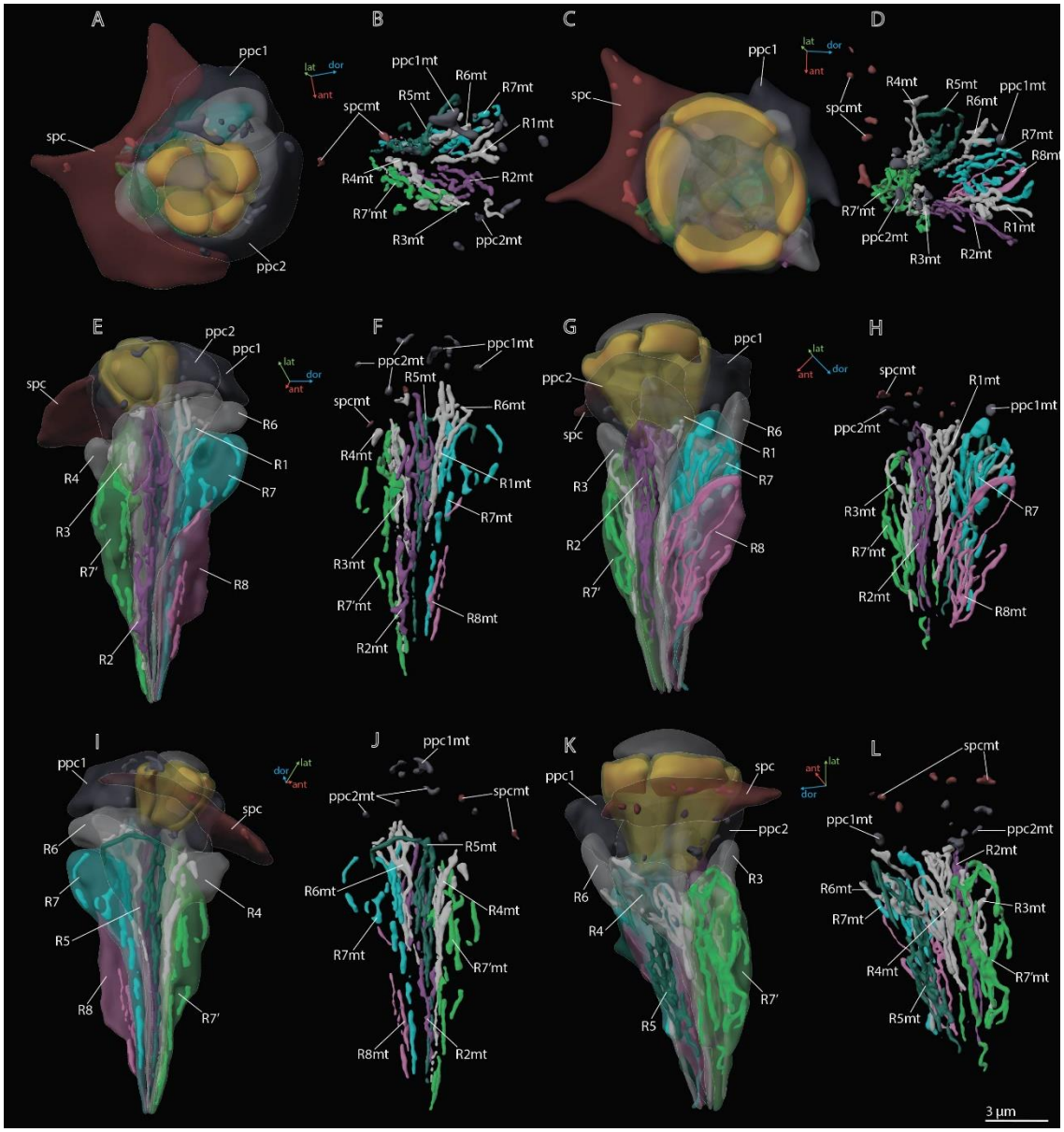

Figure 6. 3D reconstruction of mitochondria in the ommatidia cells of *M. viggianii*. A, B, E, F, I, J. DRA ommatitida (B6); C, D, G, H, K, L. Non-DRA ommatidia (C4). Abbreviations: ppc1, 2 – primary pigment cells; ppc1mt, ppc 2mt – mitochondria of PPC; R1–R8 – retinal cells; R1pg–8pg – mitochondria of retinal cells; spc –secondary pigment cells; spcpg – mitochondria of secondary pigment cells. Colors of mitochondria same as colors of their cells.

Nine retinula cells form the fused rhabdom of *M. viggianii* (Figure 3). The rhabdomere of R7 is replaced by the rhabdomere of R8 approximately in the center of ommatidium length in Non-DRA ommatidia (Figure 3K) and in the proximal third in DRA ommatidia (Figure 3F) (Suppl. 1C). The distal diameter (under the cone) is 2.0 ± 0.16 µm in DRA ommatidia and 2.7 ± 0.26 µm in Non-DRA ommatidia. The cross-section of distal rhabdom in DRA ommatidia is nearly oval in the first half of the rhabdom, and becomes rectangular in the center of ommatidium length (Figure 3D–F) (Suppl. C, see Figure 2 of DRA ommatidia). The cross-section of Non-DRA ommatidia has a strongly spherical shape (Figure 3J–L) (Suppl. C, see Figure 2 of Non-DRA ommatidia). The orientation of microvilli in

long photoreceptor cells (R7 and R7') of DRA ommatidia are orthogonal to each other and consistent throughout all rhabdom length (Chua et al., 2023). The length of the rhabdom is nearly equal in DRA and Non-DRA ommatidia, 13.4 ± 0.64 µm and 14.2 ± 1.8 µm, respectively (Table 1).

The soma of the retinula cells is filled with densely packed pigment granules (Figure 2F, 5), which can be rarely visualized in the cell's projections not far from the basement membrane. The pigment granules of the retinula cells have an elongated nearly oval shape, with the longest extension parallel to the ommatidium length (Figure 3, 5). The number of pigment granules per cell varies from 70 to 273 and depends on the volume of PR (Suppl. 2 Table 2). The mean volume of a retinula cell pigment granule is 0.049 ± 0.019 μm^3.

The distal region of cells contains rather more mitochondria profiles than the proximal region (Figure 3; 6; Suppl. 1C). In retinula cells of DRA ommatidia, the mitochondria are elongated and have numerous units (Figure 6). In non-DRA ommatidia, the mitochondria are mostly dendriform. The volume of the chondriome varies from 0.47 μm^3 to 4.03 μm^3 (Suppl. 2 Table2).

No tracheoles are present in the retina.

2.2.5. 'Ectopic' photoreceptors (ePR)

We found near the dorsal margin of the eye three 'ectopic' photoreceptor cells (per eye), each of which has several minute rhabdomeres: eight in ePR1, nine in ePR2, and 12 in ePR3 (Figure 7B, C, D). These cells are situated in the retinal area, behind the first row of DRA ommatidia: ePR1 over D7 and E7, ePR2 over B6, and ePR3 over A5 (Figure 7A, C, D), beneath the cuticle and pigment cells. The ePR have no dioptric apparatus of their own and no connection with the dioptric apparati of the adjacent ommatidia. All three cells are drop-shaped and are situated at a distance from each other (do not touch each other). The mean volume of ePR cell is 25.1 ± 1.4 μm^3 (Table 4). In the distal part, a large nucleus is situated, its volume being 7.9 ± 0.73 μm^3. The mitochondria in ePR are dendriform (Figure 7B). The mean volume of the chondriome is 1.9 ± 0.19 μm^3. All three cells have their own pigment granules, which resemble in shape and size the pigment granules of retinal cells (Figure 7B). The mean volume of pigment granules is 0.49 ± 0.17 μm^3. The axons of the 'ectopic' photoreceptors form a bundle and do not project in the lamina, reaching the medulla directly from the eye (Chua et al., 2023).

Table 4. Volumes (μm^3) and number for ePR in *M. viggianii.* EPr1–3 – ectopic photoreceptors.

	Soma	Nuclei	Rhabdomeres (total volume)	Pigment granules (total volume)	Number of pigment granules per cell	Mitochondria total volume	Number of mitochondria per cell
ER1	26,5	8,8	2,5	2,8	117	1,8	5
ER2	25,1	7,5	2,4	3,2	130	2,2	5
ER3	23,6	7,6	2,2	3	105	1,9	10
Mean	25.1 ± 1.4	7.9 ± 0.73	2.4 ± 0.15	2.9 ± 0.22	117 ± 12	1.9 ± 0.19	7 ± 3

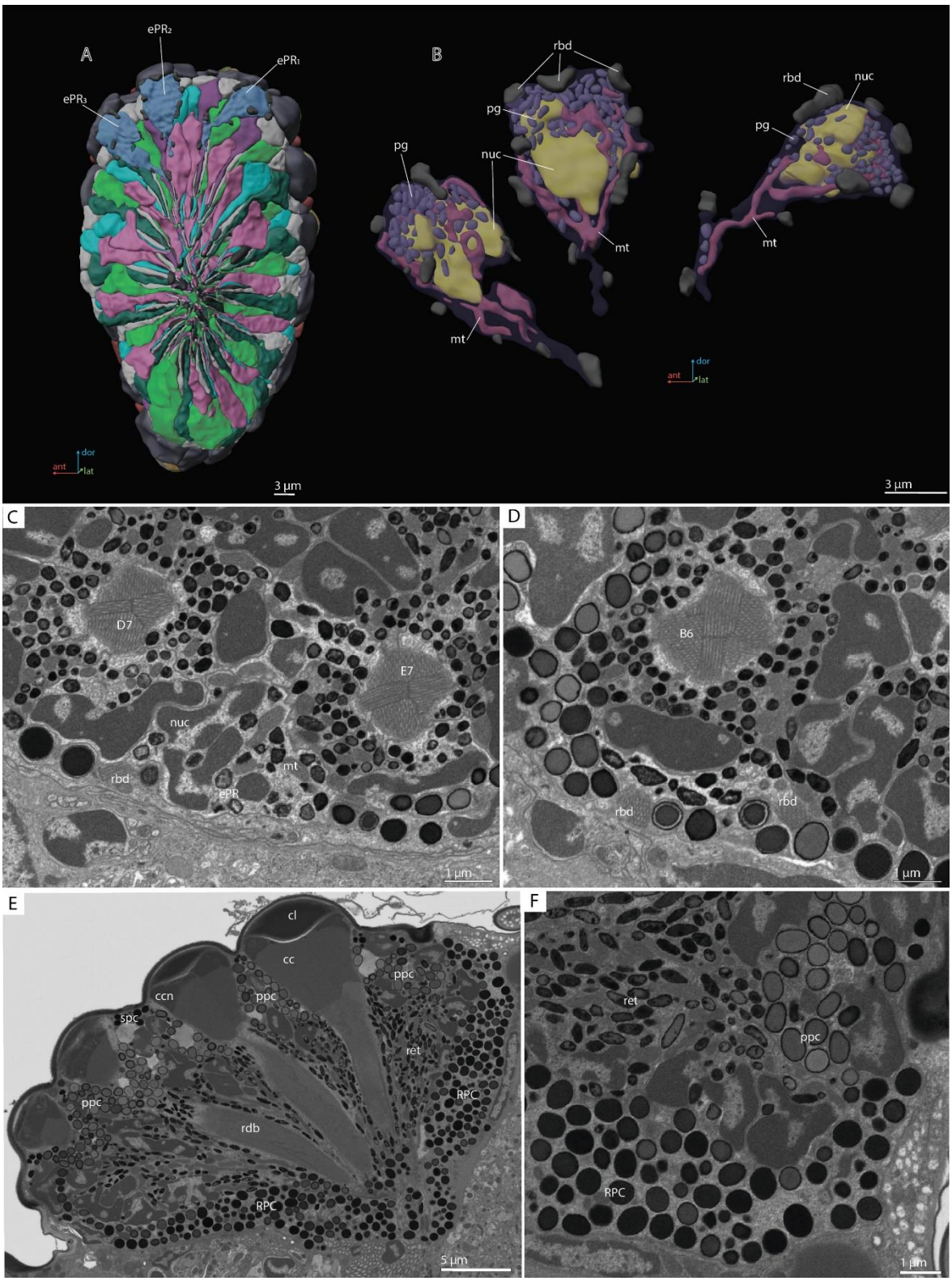

Figure 7. Ectopic photoreceptors and a rind photoreceptor shield in the compound eye of *M. viggianii*. A. A 3D reconstruction of the eye: posterior view from of the retinal area with labeled ePRs; B. A 3D reconstruction of ePRs; C, D. An EM section through dorsal border of the eye; F. An EM section through the eye showing RPC. Abbreviations: cc – crystalline cones; cl – corneal lens; ePR1-3 – ectopic photoreceptors; mt – mitochondria; nuc – nuclei; pg – pigment granules; ppc – primary pigment cells; rbd – rhabdomeres; spc – secondary pigment cells. B6, D7, E7 – DRA ommatidia abutting ePR.

2.2.6. Rim pigment cells

The eye is surrounded by 16 rim pigment cells (RPC), which are morphologically similar to primary pigment cells (Figure 2F, 7E, F). Although they have not been reconstructed because identifying their boundaries is difficult, their number was determined by counting the nuclei surrounding the eye. RPCs are filled with pigment granules of spherical shape. The mean volume of one pigment granule is 0.18 ± 0.049 μm^3.

3. Discussion

The general structure of the compound eye in *M. viggianii* is similar to that previously described in *M. polilovi,* which had been identified earlier as *M. mymaripenne* (Makarova et al., 2015) and subsequently described as a new species (Polaszek et al., 2022). In contrast to oblong and 'narrow' ommatidia in the eyes of other minute hymenopterans (Fisher et al., 2011; Makarova et al. 2015; Fisher et al., 2019) ommatidia in *M. viggianii* are short and 'wide'.

3.1. DRA and non-DRA ommatidia

The results of the 3D reconstruction, morphometry, and volumetry of the key components of the eye and data on the connectome of the lamina (Chua et al., 2023) have shown considerable differences (corneal and retinal) between DRA and non-DRA ommatidia (Table 5). Morphometric analysis clearly reveals a group of seven ommatitia (D7, E7, B6, C6, D6, A5, and B5) in the dorsal area of the eye (DRAm) (Table 1, 2; Figure 2A). The analysis of synaptic connections of R7 and R7' supplements this group with three more ommatidia (E6, C5, and A4) (DRA(+)) (Chua et al., 2023) (Figure 2A; Suppl. Table 1, 2). According to their morphological characters, the ommatidia DRA+ have features of both DRAm ommatidia and non-DRA ommatidia. Judging by the size of the cone and lens and by the position of the nuclei in the cells of the cone, ommatidium E6 is more similar to DRAm ommatidia (Figure 2; Suppl. Tables 1, 2). The nuclei occupy almost the entire cell volume in DRAm ommatidia. In two other ommatidia, DRA+ (C5 and A4), the dioptric apparatus is more similar with that of non-DRA ommatidia (the nuclei of the cone cells form an aperture under the lens and are situated in the dorsal third of the cells). The volumetric parameters of DRA+ ommatidia are slightly greater than those of DRAm ommatidia but smaller than those of non-DRA ommatidia (Table 2). The morphology and the retinotopic pattern of ommatidial specialization in the eye suggest that DRA+ ommatidia lie in the transitional zone between specialized and non-specialized ommatidia.

Specialized ommatidia of DRAs in the compound eyes were described in many insects (Odonata, Orthoptera, Hemiptera, Coleoptera, Hymenoptera, Lepidoptera, Diptera, and others; summarized in Labhart, Meyer, 1999; Labhart et al., 2009). The results of our morphological analysis of all ommatidia in *Megaphragma* are consistent with the light-polarization related features in Hymenoptera and other insects (e.g., Gribakin, 1972; Menzel, Snyder, 1974; Schinz, 1975; Labhart, 1980; Aepli et al., 1985; Menzel et al., 1991; Labhart, Meyer, 1999; Wehner, Labhart 2006; Greiner et al., 2007; Narendra et al., 2013). Moreover, it agrees well with the regional specialization of DRA ommatidia manifested in the orientation of microvilli and synaptic connectivity in lamina cartridges (Chua et al., 2023).

Table 5 Features of DRA and Regular ommatidia obtained by reconstruction of compound eyes of *M. viggianii*. DRA – dorsal rim ommatidia in general (DRAm and DRA+); DA – dioptric apparatus; PC – pigment cells; PPC – primary pigment cells. t-test * 0.001 ≤ p < 0.01, ** 0.0001 ≤ p <0.001, *** p < 0.0001.

Ommatidial area	Features		DRA	non-DRA	Difference
	Ommatidial length, µm		19.2 ± 0.37	22.3 ± 2.5	**
DA	Cone	Length, µm	3.0 ± 0.37	4.6 ± 0.59	***
		Wigth, µm	4.5 ± 0.21	6.6 ± 0.25	***
		Volume, µm^3	13.0 ± 6.0	32.9 ± 5.9	***
	Lense	Lense diameter, µm	6.9 ± 0.89	8.0 ± 0.77	*
		Volume, µm^3	16.5 ± 14.0	41.4 ± 9.0	**
		Lense thickness, µm	2.5 ± 0.56	3.3 ± 0.39	*
		Inner curvature, µm	1.2 ± 0.32	3.0 ± 0.51	***
		Outer curvature, µm	3.3 ± 0.63	4.7 ± 0.39	***
	Cone cell (CC) nuclei	CC nuclei	Fill most of the volume of the cell	Form a ring in the upper third of the cone	-
		% of cone volume	58 ± 0.17	23 ± 0.02	***
		Volume, µm^3	6.6 ± 0.68	7.5 ± 1.1	***
PC	PPC volume		47.1 ± 14.3	64.5 ± 11.4	***
Retina	Rhabdom	Shape	Rectangular shape of rhabdom from center to lower part	Spheric shape of the rhabdom along whole length	-
		Diameter, µm	2.0 ± 0.16	2.7 ± 0.75	***
	Microvilli orientation		Orthogonal orientation of R7, R7' microvilli along the rhabdom length	Non-ortogonal orientation of R7, R7'	-
	Volume, µm^3	Duet (R2, R5)	24.8 ± 3.9	30.3 ± 3.2	***
		Quartet (R1, R3, R4, R6)	17.8 ± 1.9	21.4 ± 3.5	***
		R7'	33.0 ± 2.5	53.3 ± 11.1	***
		R7, R7'	32.6 ± 3.7	41.9 ± 15.1	***
		R8	15.8 ± 1.9	28.2 ± 4.2	***

3.1.1. Corneal specializations

There is a significant difference in the length and volume of DA between DRA and regular ommatidia (Tables 1, 2, 5). The lenses in DRA ommatidia are visually different from those in regular ommatidia (Figs. 2, 4). Considerable differences are visible in the diameter, thickness of the cornea, radius of curvature (Figure 8D), and volume of the lenses, which are smaller in DRA ommatidia (Suppl. 2 Table 4).

DRA ommatidia are characterized by smaller DA, lenses, and cone cells than regular ommatidia (Tables 1, 2). The nuclei of the cone cells of DRAm ommatidia (and those of ommatidium E6 of DRA+) occupy almost the entire cell volume. The chromatin of the nuclei is strongly compacted and occupies almost all volume of each nucleus (Figure 3). Since the cone cells are adjacent to each other over their entire length, their nuclei form an electron-dense formation under the lens (Figs. 3, 4) (Suppl. 1C). Chromatin inside the cell nucleus has a direct effect on light propagation, so that the

nuclei act as extra collecting lenses, as was reported for rod cells of nocturnal vertebrates (Solovei et al., 2009; Błaszczak et al., 2014). Since the nuclei in regular ommatidia are arranged differently in cone cells, we suggest that the nuclei of the cone cells of DRA ommatidia in *M. viggianii*, when combined under the lens, also perform the function of augmenting the proposed optical effect, reducing the scattering of light, and possibly acting as a light filter, facilitating the specialization of this group of ommatidia. The data obtained are indirectly confirmed by the difference in calculated focal lengths (Figure 8E), which are smaller in DRA (and intermediate in E6, which has a similar cone structure) than in non-DRA ommatidia.

The volume of the lenses and of the cone cells also supports the division into the areas DRAm and DRA+ (Table 2; Figure 8F).

3.1.3. Retinal specializations

The group of short PRs (R1–R6) is clearly divided into the duplet (R2, R5) and quartet (R1, R3, R4, R6), according to the volume of the cells, which agrees with the data on lamina circuits (Chua et al., 2023) and other data (Friedrich et al., 2011). Volumetric analysis of PR subtypes among all ommatidia and between DRA and non-DRA groups shows significant differences (Table 5). Kruskal–Wallis test for all ommatidia shows H (3, N= 261) = 146.3, $p < 0.0001$; H (3, N = 90) = 69.36 p = .0000 for DRA and H (3, N = 171) = 106.1, p = 0.000 for non-DRA. The smaller volume among the short PRs belongs to the quartet (17.8 ± 1.9 μm^3 and 21.4 ± 3.5 μm^3 for DRA and non-DRA ommatidia, respectively). The duplet PR has a mean volume of 24.8 ± 3.9 μm^3 in DRA and 30.3 ± 3.2 μm^3 in non-DRA ommatidia. The greater volume among PRs belongs to R7' cells and is 33.0 ± 2.5 μm^3 in DRA, and 53.3 ± 11.1 μm^3 in non-DRA ommatidia. The basal PR cell, R8, has a volume of 15.8 ± 1.9 μm^3 in DRA and 28.2 ± 4.2 μm^3 in non-DRA ommatidia.

Rhabdom volume gradually increases from the dorsal to the ventral area of the eye (Figure 8A; Suppl. 2 Table 2). The volumes of the rhabdomeres of the photoreceptor in all ommatidia of the eye vary (Table 2) and reveal a general trend for an increase with total cell volume. The rhabdomeres of cells R7' and R8 are much smaller in DRA ommatidia than in non-DRA ommatidia (Figure 8B, C) (Table 2). Opposing twin rhabdomeres R7 and R7' do not show any significant differences in volumes (Table 2), but orthogonal orientations of their microvilli support the role played by DRA in detecting light polarization (Chua et al., 2023). Analysis of the orientation of the microvilli of the rhabdom have shown that in DRA ommatidia rhabdomeres of the R7 and R7' cells are consistent throughout the depth of the ommatidium and orthogonal to each other, which is consistent with the disparity in the numbers of synapses received by R7 and R7' in the lamina (Chua et al., 2023).

In spite of the difference in length between DRA and non-DRA ommatidia, the length of the rhabdoms in the ommatidia differs little: 13.4 ± 0.64 µm for DRA and 14.2 ± 1.8 µm for non-DRA, which is much smaller than in *Apis mellifera* (200–500 µm) (Menzel et al., 1991), and comparable with that of *Trichogramma evanescens* (18.3 ± 0.28 µm) (Fisher et al., 2019). The total rhabdom shortening in *M. viggianii* ommatidia probably favors polarization and absolute sensitivity, by reducing self-screening, and widening the rhabdomeric cross-sectional area (Nilsson et al., 1987; Labhart, Meyer, 1999 Homberg, Peach, 2002).

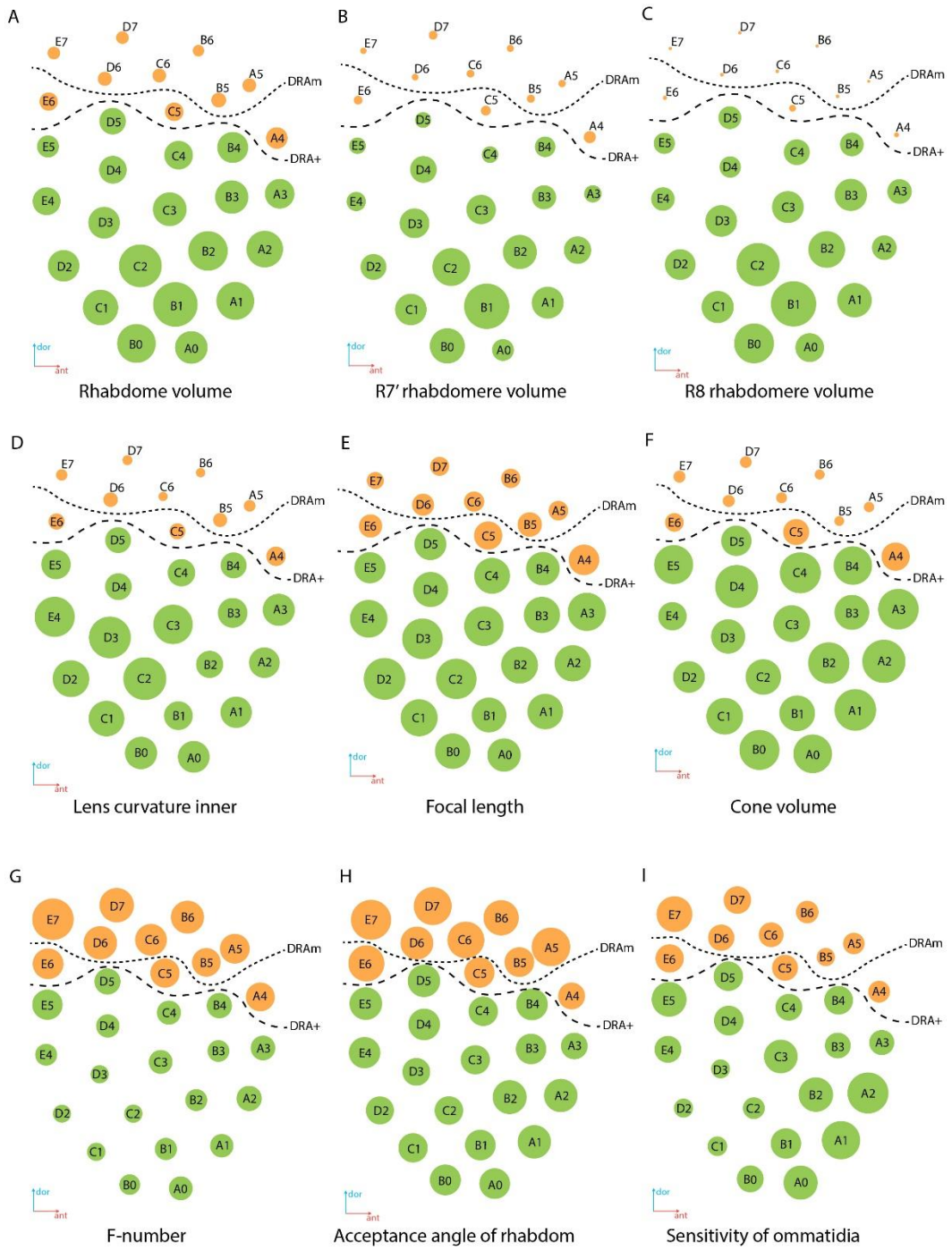

Figure 8 Regional specialization of the compound eye in *M. viggianii*. Bubble size indicates the value of each parameter. A. The rhabdom volume; B. The volume of rhabdomere R7'; C. The volume of rhabdomere R8; D. The inner curvature of the lens; E. The focal length; F. The cone volume; G. The f-number; H. The acceptance angle of the rhabdom; I. The sensitivity of the ommatidium. DRAm – dorsal rim area ommatidia (morphological specialization); DRA+ – transitional zone ommatidia. Ommatidia are named as in Chua et al. (2023).

The cross-sections of the distal rhabdom in DRA and non-DRA ommatidia differ. Rhabdoms in DRA possess partly rectangular cross-sectional profiles (Figure 3) (Suppl. 1C), similar to the profiles of polarization of sensitive ommatidia in the DRA of ants and bees (Gribakin, 1972; Menzel et al., 1991; Labhart, Meyer, 1999; Greiner et al., 2007). In the DRA ommatidia of *M. viggianii,* the rhabdom

cross-section shape is not constant throughout its length. In the first half (under the lens) the shape of the rhabdom is nearly round, and becomes rectangular or nearly square in the center (Figure 3D–F) (Suppl. C, see Figure 2 of DRA ommatidia). Non-DRA ommatidia possess round profiles over the entire length of the rhabdom (Figure 3J–L) (Suppl. C, see Figure 2 of Non-DRA ommatidia).

In DRA ommatidia rhabdoms have smaller volume and narrower distal parts than in non-DRA ommatidia (Suppl. 2 Table; Suppl. 1C).

3.1.4. Optical properties of DRA

Some optical parameters differ between ommatidia within the eye (Figure 8E, G, H, I). (Suppl. 2 Table 4). The short focal length in DRA (Figure 8E) in combination with rhabdom diameters results in the relatively large acceptance angles of the rhabdoms (Figure 8H). Ommatidia located across the diagonal area of the eye are more sensitive to light (Figure 8I). Estimated optical sensitivity of the eyes very close to those reported for diurnal hymenopterans with apposition eyes (Greiner et al., 2004; Gutiérrez et al., 2024) and possess around 0.19 ± 0.04 μm^2 sr. *M. viggianii* have reasonably huge values of acceptance angle Δρ, and thus should results in a low spatial resolution (Suppl. 2 Table 4).

3.2. Other findings

3.2.1. Retinula cells and rhabdom

Despite the extreme miniaturization of the eye leading to the dense packing of ommatidia components and lack of space, traces of structural diversification of PRs are retained and indicating a strong evolutionary conservation. Morphological differences of photoreceptors as a key to spectral sensitivity cells were supposed by Gribakin (1975). The division into the duet and quartet PRs is an ancestral trait of the insect retina (Friedrich et al., 2011). The position of the nuclei of the outer PR quartet (R1, R3, R4, and R6) is different from that of the duet (R2 and R5) and from that reported for bees (Gribakin, 1975), ants (Herrling et al, 1976), beetles (Schmitt et al., 1982), dragonflies (Meinertzhagen et al., 1983), and butterflies (Awata et al., 2009). The most distal position of the nuclei of the outer PR quartet relative to the duet is also found in *Megaphragma* (Figure 4F, H, J, L). Such differences between cells are an indication of the strong evolutionary conservation of the outer PR quartet and duet subgroups and can be attributed to their wavelength sensitivities (Friedrich et al., 2011).

In *Megaphragma* the PRs duet projects deeper into the lamina than the quartet PRs, as in most Hymenoptera (Ribi, 1975; Greiner et al., 2004). Duet and quartet PR also have different arrangements in axon bundles and numbers of output synapses in the lamina: duet synapses are distributed over the whole length of the lamina cartridge, but quartet synapses are distributed in the anterior part of the cartridge (Chua et al., 2023). It has been suggested that the outer PR duet provides information for motion-detecting vision, while the quartet PRs participate in color vision (Takemura, Arikawa, 2006).

Morphological analysis of the ommatidia showed that in most ommatidia the cytoplasm and the rhabdomere of R7 are distinguished by a lower electron density than adjacent cells (Supl. 1 C). This may be the result of accidental bleaching of the long wave receptors during fixation of the sample and of the reaction of OsO_4 as a 'developer' of light-induced changes in cells (Gribakin, 1975). Retinula cells R7 and R7' have been reported as UV sensors in hymenopteran ommatidia (Wakakuwa et al., 2007; Spaethe, Briscoe, 2005). This can indirectly explain the relatively larger volume of R7'

cells and rhabdomeres, and the highest pigment granule volumes in R7 and R7' compared with other retinula cells in the eye of *Megaphragma*. This agrees well with the connectivity pattern findings in the lamina (Chua et al., 2023).

The volume and number of pigment granules and mitochondria per cell positively correlate with the volume of PR (Tables 2, 3). The presence of numerous mitochondrial profiles visible in most single-sections in the distal part of ommatidia is a result of the sectioning of few dendriform-like units, rather in non-DRA than in DRA ommatidia (Figure 3, 5). The distal parts of the cells are referred to as the most active metabolically, thus indicating an exponential gradient of light absorption (Gribakin, 1976).

3.2.2. Pigment cells

The volume of PPC and SPC is greater in DRA ommatidia than in non-DRA ommatidia (Table 2). The shapes and volumes of pigment granules differ in PPC, SPC and PR (Figure 2F, 3, 7E, F). The pigment granules of all cell types also vary in electron density. PPC have lower electron density than SPC and granules of PR (Figure 6). This difference in electron density could be an indication of different biochemical activity and shielding functions of light-absorbing pigment granules (Gribakin, 1981).

The total volume of pigment granules is higher in pigment cells than in photoreceptor cells. Pigment granules occupy about 32% of PPC and 26% of SPC volume. In contrast, pigment granules of the retinal cells occupy 10–13% of cell volume.

A total of 24 SPC were identified in the whole eye of *M. viggianii*. However, we cannot clearly 'link' them with any particular ommatidium because they probably perform their screening function for adjacent ommatidia (Figure 2A, F). Pigment granules of SPC vary in shape in different parts of the eye. Preliminary observations shows that the SPC near the DRA ommatidia have round pigment granules (Figure 5B). The SPC that surround the area of non-DRA ommatidia in the center and proximal third of the eye have more oval pigment granules (Figure 5D).

16 RPC ensheathe the eye laterally and prevent light from passing from areas outside the compound eyes onto the photoreceptors (Meyer-Rochow, 1999; Stavenga, 1989, 2002; Tomlinson, 2012; Mohr et al., 2020). In spite of the same volume and shape of granules in PPC and RPC, the RPC pigment granules have a high electron density, comparable to SPC (Figure 7E, F). Studies on *Drosophila* have shown that the pigment rim originates from secondary/tertiary-like pigment cells of the pupa (Wolff, Ready, 1991).

3.3. Comparison with Trichogramma

The complete cellular level 3D reconstruction of the entire eye of one of the smallest insects provides the most detailed information about the structure of the insect compound eyes in general. However, the uniqueness of the dataset complicates an extensive comparative assessment of the results, in particular the volumetric ones. Yet, there exists a pioneering 3D reconstruction of three ommatidia from the eye of a male *Trichogramma evanescens* Westwood, 1833 by Fischer et al. (2019). Considering that the data for *T. evanescens* was obtained from the central ommatidia (Fischer et al., 2019), we can tentatively assume that they were non-DRA.

Table 6 Comparison of volumes (µm^3) of ommatidial components for *Trichogramma evanescens* and *M. viggianii*. Data on *T. evanescens* are from Fischer et al. (2019). CC – crystalline cones R1–R8 – retinal cells; PPC – primary pigment cells; SPC – secondary pigmen cells.

	Soma											
	CC	PPC	SPC	R1	R2	R3	R4	R5	R6	R7'	R7	R8
T. evanescens	12.3 ± 1.2	40.5 ± 6.9	21.0 ± 2.5	18.5 ± 2.3	27.6 ± 0.35	20.3 ± 1.3	18.2 ± 1.4	26.9 ± 1.8	17.5 ± 0.92	19.7 ± 4.3	26.5 ± 2.8	8.48 ± 1.1
M. viggianii (B3, C3, C4)	32.9 ± 7.5	61.8 ± 9.2	23.2 ± 3.8	20.4 ± 0.81	30.3 ± 3.0	19.4 ± 1.8	21.2 ± 1.6	30.2 ± 2.0	18.1 ± 1.7	48.4 ± 8.4	33.8 ± 10.9	26.9 ± 1.7
M. viggianii (all regular)	32.9 ± 5.9	64.4 ± 11.4	24.5 ± 3.1	20.9 ± 3.2	29.4 ± 3.1	22.0 ± 2.6	22.3 ± 3.5	31.1 ± 3.2	20.4 ± 4.5	53.3 ± 11.1	30.6 ± 8.5	28.1 ± 4.3
	Nuclei											
T. evanescens	3.1 ± 0.18	3.6 ± 0.29	3.2 ± 0.40	2.4 ± 0.09	2.4 ± 0.15	2.4 ± 0.17	2.1 ± 0.11	2.2 ± 0.24	2.3 ± 0.1	2.4 ± 0.3	2.9 ± 0.48	1.9 ± 0.15
M. viggianii (B3, C3, C4)	7.0 ± 1.0	7.2 ± 1.1	5.7 ± 0.28	7.0 ± 0.11	7.9 ± 0.18	6.7 ± 0.63	6.9 ± 0.65	8.0 ± 0.48	5.9 ± 0.36	9.1 ± 1.1	8.1 ± 1.3	8.3 ± 0.73
M. viggianii (all regular)	7.5 ± 1.1	7.6 ± 0.98	6.4 ± 1.03	7.0 ± 0.56	7.6 ± 0.90	7.2 ± 0.72	7.2 ± 0.84	7.9 ± 0.71	6.5 ± 1.7	9.2 ± 1.0	7.9 ± 1.2	8.3 ± 0.80
	Rhabdomere											
T. evanescens	n/a	n/a	n/a	2.4 ± 0.2	3.5 ± 0.19	2.2 ± 0.02	2.3 ± 0.08	3.5 ± 0.15	2.4 ± 0.25	2.1 ± 0.27	3.8 ± 0.28	0.79 ± 0.07
M. viggianii (B3, C3, C4)	n/a	n/a	n/a	3.7 ± 0.92	6.0 ± 0.79	2.3 ± 1.0	3.2 ± 0.46	5.9 ± 0.54	2.8 ± 0.071	11.1 ± 3.0	6.5 ± 2.3	6.6 ± 0.80
M. viggianii (all regular)	n/a	n/a	n/a	4.1 ± 1.6	5.6 ± 1.3	3.2 ± 0.94	3.6 ± 1.3	5.9 ± 0.97	3.2 ± 0.74	12.7 ± 3.9	5.5 ± 2.1	6.7 ± 1.6
	Nuclei/Soma, %											
T. evanescens	25.0 ± 2.7	9.1 ± 1.2	15.2 ± 2.5	13.0 ± 1.1	8.8 ± 0.55	11.6 ± 0.67	12.4 ± 1.6	12.0 ± 0.41	8.1 ± 0.44	13.3 ± 1.02	11.0 ± 1.02	23.0 ± 1.3
M.viggianii (B3, C3, C4)	22.5 ± 7.1	11.7 ± 1.7	25.0 ± 4.5	34.4 ± 1.7	26.5 ± 3.3	34.7 ± 1.0	19.0 ± 0.98	32.4 ± 1.2	26.6 ± 0.33	32.9 ± 1.3	25.1 ± 6.8	30.8 ± 0.74
M. viggianii (all regular)	35.3 ± 19.9	15.1 ± 11.6	28.6 ± 7.9	34.5 ± 3.4	27.1 ± 2.9	34.4 ± 3.1	20.1 ± 4.2	34.2 ± 3.5	27.0 ± 3.1	33.5 ± 6.2	26.7 ± 4.6	34.8 ± 7.8

In general, the eyes of *Megaphragma* are smaller than those of *Trichogramma*, and contain at least 4 times fewer facets (Makarova et al., 2015). But individual facets of *Megaphragma* eyes have a wider diameter of lenses than those of *Trichogramma* eyes. The small number of ommatidia in *Megaphragma* in comparison to *Trichogramma* is probably compensated by the larger diameter of the facets, wider and shorter rhabdoms, and short DA (Makarova et al., 2025).

The location of the nuclei in the duplet (R2, R5) and R7 equivalent cells (R7, R7’) differ in *Trichogramma* and *Megaphragma*. In *T. evanescens* the nuclei of the duplet occupy a proximal position approximately half-way along the ommatidia, and the nuclei of R7 and R7’ cells are shifted ventrally to the level slightly above that for the duplet (Fischer et al., 2019). In *Megaphragma*, the nuclei of the duplet are similar or more distal compared to that in R7 and R7’ (Figure 4).

3.3.1. Number of SPCs

The main structural difference between *Megaphragma* and *Trichogramma* ommatidia is the number of SPCs. According to the description of *Trichogramma* ommatidia, six (Fisher et al. 2011) or five (Fischer et al., 2019) SPC are positioned directly beneath the cornea and envelop PPCs in their dorsal third (Fischer et al., 2019). There is no information about the total number of SPCs in the eye of *Trichogramma* or any other insect. In the *Megaphragma* right eye there is a total of 24

SPCs. According to 3D reconstructions, only the PPCs of the central rows of ommatidia can be 'encircled' by four SPC; the outer rows are abutted by two or three SPCs. The reduction of the number SPC could be a result of miniaturization in the *Megaphragma* eyes.

3.3.2. Mitochondria

The second structural difference is the absence of mitochondria in cone cells of the *Megaphragma* ommatidia which are present in *Trichogramma* (Fisher et al., 2019). Although the cones of *Megaphragma* do not contain bona fide mitochondria, we found electron-dense elements, which could be residual bodies, near the border of the cone cells, where the mitochondria of *Trichogramma* were reported (Figure 3G, I; Suppl. 1C (A3, C4, B3)).

There are also differences in the shape and number of mitochondria in the retinal cells. In *Trichogramma* there are elongated mitochondria in the PR cells, but in *Megaphragma* most of the mitochondria are dendriform.

Finally, the total volume of mitochondria in retinula cells is higher in *Trichogramma* than in *Megaphragma* (Table 3).

3.3.3. *Pigment granules*

Despite the smaller volume of cells, *Trichogramma* has a higher number of pigment granules in PPC/SPC (212 ± 50/255 ± 16) (Fischer et al., 2019) than *Megaphragma* (about 158 ± 29/144 ± 52). The mean volume of individual pigment granules differs between the two genera. The mean unit volume in *Trichogramma* SPC is 0.017 ± 0.03 μm^3 (Fisher et al., 2019) and 0.050 ± 0.016 μm^3 in *Megapragma*. The mean unit volume in PPC granules is greater in *Trichogramma* (0.52 ± 0.1 μm^3) (Fisher et al., 2019) than in *Megapragma* (0.18 ± 0.039 μm^3). The total volume of pigment granules of pigment cells is greater in *Megapragma* than in *Trichogramma* (Table 3). However, the measurements of Fischer and his co-authors contain some discrepancies in the values of the general volumes of pigment granules, which cannot be so small given the number and diameter of the pigment granules of PPC (Fischer et al., 2019).

The number of pigment granules in the retinal cells in *Megaphragma* (from 70 to 270 and depending on the cell size and ommatidia type (Dra of Non-DRA)) is higher than in *Trichogramma* (40 to 80, depending on cell size) (Fischer et al., 2019) (Suppl. 2 Table 2). Despite this, the total volume of pigment granules per cell is rather close in *Megaphragma* and *Trichogramma* (Table 3).

Despite the similar volume of the R7 cells, the total volume of pigment granules in the R7 cells in *Megaphragma* is almost twice as great as in *Trichogramma* (Table 3). As in *Trichogramma,* the R7' and R7 cells in *Megaphragma* display a higher pigment granule volume in comparison to those of other photoreceptors, which could indirectly implicate them as UV sensors (Wakakuwa et al., 2007; Spaethe, Briscoe, 2005). But in *Megaphragma* R7 does not have a high rhabdomere volume (whereas R7' does have a high volume), in contrast to *Trichogramma,* in which R7' does not stand out among other retinula cells (Table 6). This difference could be a result of the functional diversification between R7 and R7' in different species or expression of different opsin paralogs in the same ommatidia (Friedrich et al., 2011).

3.3.4. Volumetry

In addition to revealing morphological differences of ommatidia, we compared their volumes in two ways: we compared the three ommatidia studied in *Trichogramma* with three central ommatidia of *Megaphragma* (B3, C3, C4) and with all non-DRA ommatidia of *Megaphragma* (Table 6).

Despite having smaller eyes and body length (~290 µm) and fewer ommatidia, *M. viggianii* cells have 0.9–3.3 times greater volume compared to *T. evanescens,* which has body length of 400–500 µm (Table 6). The most prominent difference in volume was revealed between the R8 PRs (more than 3 times larger in *Megaphragma* as in *Trichogramma*), the R7' PRs (2.5 times larger in *Megaphragma*) and the cone cells (2.5 times larger in *Megaphragma*). The minor difference between the majority of retinal cells can be explained as a result of the slimmer ommatidia of *Trichogramma* eyes, or by the sex differences: *Trichogramma* males have smaller eyes and shorter ommatidia than females (Fischer et al., 2011, 2019).

The volumes of the nuclei in all cells of the *Megaphragma* ommatidia are 1.7 to 4.2 times greater than in *Trichogramma* photoreceptors (Table 6) and interneurons (Fisher et al., 2018), despite the smaller difference in body size. The percentages for cell volume (soma) occupied by the nuclei in non-DRA ommatidia of *Megaphragma* are higher than in *Trichogramma*, consituting up to 23% in cone cells, 12% in PPC, 25% in SPC, and 19–34% in PR (Table 6). The mean nucleus volume in the ommatidium cells of *Megaphragma* is also similar to the nucleus volume of most Johnston's organ cells (Diakova et al., 2022). *Megaphragma* nuclei are also characterized by the more compacted chromatin. The greater volume of nuclei in spite of the smaller eyes can be explained by the fact that *M. viggianii* has one of the largest genome sizes in Chalcidoidea (Sharko et al., 2019).

4.3. 'Ectopic' photoreceptors (ePR)

We have revealed for the first time the description photoreceptor cells that are not connected with the dioptric apparatus of the eye (Figure 7). The presence of such cells is confirmed in stacks of three heads of *Megaphragma* (two females and one male). The number of cells in all samples is invariably three. Tracing the projections of these 'ectopic' photoreceptors demonstrate that their axons form a bundle, do not project into the lamina, and reach the medulla directly from the eye. In the lamina, they squeeze between two cartridges before projecting the medulla (Chua et al., 2023). Their morphology is closer to those of R8 than to those of any other cell type. Although these ePR axons lack corresponding LMCs, they exhibit similar ramification and projection into the medulla as R8, and even form connections with cells that synapse with R8 in other medulla columns (Chua et al., 2023). Having no cone or lens, their small rhabdomeres may receive unfocused light. This could potentially be used to measure ambient light intensity and may be helpful in regulating circadian rhythms (Chua et al., 2023).

Conclusion

Despite the extremely small body size, the compound eyes of *M. viggianii* retain an almost complete set of the cellular components of the ommatidia. The compound eye exhibits a regional specialization of ommatidia (DRA) putatively capable of polarized light perception. Ommatidia within the eye differ considerably in size and shape, and demonstrate corneal and retinal specializations. The results of the 3D reconstruction, morphometry, and volumetry of the key components of the ommatidia show a good match with the lamina connectivity patterns (Chua et al., 2023). A transitional zone is present between the adjacent regular ommatidia of central area of

the eye and DRA. Despite the nearly anucleate nervous system, the main sensory organs (such as the compound eye or Johnston's organ) and the retrocerebral endocrine complex of *M. viggianii* retain all their nuclei (Diakova et al., 2021; Desyatirkina et al., 2023). Our results not only reveal the general principles of the miniaturization of compound eyes but also provides context for future interpretation of the visual connectome of *M. viggianii*.

Methods

Material. Adult females of *Megaphragma viggianii* Fusu, Polaszek & Polilov 2022 (Hymenoptera: Trichogrammatidae) were reared from eggs of *Heliothrips haemorrhoidalis* (Bouché, 1833) (Thysanoptera: Thripidae). For detailed protocol, see Polilov et al. (2021).

The head was separated from the body in a cold fixative and immediately transferred to fresh fixative of 4 °C for 1 h, which consisted of 1% glutaraldehyde (GA) and 1% osmium tetroxide (OsO4) in 0.1 M sodium cacodylate buffer (pH = 7.2). The material was then washed in the same buffer and fixed for 2 h in 2% GA in the buffer at 4 °C. Next, the material was washed in the buffer and post-fixed for 16 h in 2% OsO4 in the buffer at 4 °C. After fixation material was washed with double distillate water, and then subjected to a 1% UA solution in ddH2O overnight at 4 °C, and then placed (in the same solution) into a constant-temperature oven for 2 h at 50 °C. The specimens were then washed in ddH2O and contrasted with Walton's lead aspartate solution (2 h, 50 °C). Material was then washed in ddH2O. Subsequently, dehydration of the material was continued using ethanol and acetone. The material was then placed in a mixture of an embedding medium (Epon, Sigma) and acetone (1 : 2) for 2 h at RT, and then in 1 : 1 mixture overnight at RT, after which the samples were transferred to a pouring medium for 5 h at RT. The samples were ultimately transferred to silicone embedding molds with fresh Epon and placed in a constant temperature oven for 48 h at 60 °C.

FIB‑SEM imaging. The specimen was studied using custom FIB-SEM (Zeiss Merlin scanning electron microscope that has a Zeiss Capella focused ion beam). To image an entire head, we used 2 MHz pixel rates with a 2nA primary electron beam with final voxels that were sampling at 8 × 8 nm in x and y and milled with effective 8 nm increments. Image stack of one head was acquired. The right eye was used for the three-dimensional (3D) reconstruction, volumetric analysis and morphometry. The right eye, on which the reconstruction was performed, has a several damage regions due milling (Suppl. 1C), that hinder the complete reconstructions of lenses and cones on few ommatidia. The volumetric data of lenses and cones, some linear measurements (lens thickness, cone length, cone width, curvature radius) and to visualize the complete 3D-model of eye we use (measure or reconstruct) the elements from another eye (left). The cells of single interfacet bristles were not reconstructed, because of damaging on right eye and worst quality of section on the left.

SEM. The Bouin fixed material was gradually dehydrated through a series of ethyl alcohols 70%, 95% ethyl alcohol, each change for 30 min, 100% two changes for 30 minutes; and then acetone (100%, two changes for 15 min), critical point dried (Hitachi HCP-2) and sputtered with gold (Giko IB-3). The specimens were studied and imaging was performed using Jeol JSM-6380 with a 5-megapixel digital camera.

3D reconstruction. All cellular and subcellular elements of the eye were manually segmented with Bitplane Imaris 9.5 on right compound eye of the first specimen. The raw models were post-processed in Blender using tools of retopology and smooth. The volumes of cells and cell structures

were calculated based on the 3D models using the Imaris statistics module. Volumes of photoreceptor bodies were calculated without cell processes, as volumes of cone cells without of their projections to basement membrane. The pigment apparatus of the compound eye (the pigment granules) (Figure 1 F) were reconstructed using Ilastic software.

Morphometry. Each ommatidia was numerated for comparison between ommatidia the same eye, and right and left eye. All linear dimensions were measured on the FIB-SEM images using measurement tools of Bitplane Imaris (v9.5). For rhabdomere segmentation the extra 29 stacks of ommatidia were performed from the FIB-SEM data using a Python script (N.J.C.) (see Chua et al., 2023 Methods/Optics measurements and calculations). The rhabdomeres on each stack were segmented manually in Bitplane Imaris software. Statistical analysis was performed using STATISTICA 12, including t-tests for data analysis.

Optical calculations

To compare the optical properties of the compound eyes, the anatomical measurements were used to calculate relevant parameters: focal lengths, F-number, acceptance angle and sensitivity of ommatidia (for description the formulas and parameters, see Makarova et al., 2015; Suppl. 2 Table 4).

Identifying the retinula cells and terminology

For retinula cell numeration, we use the standardized *Drosophila*-based numbering convention (Friedrich et al., 2011) which is useful for understanding the photoreceptor subtype homologies. We combine cell body morphology (position of R8, basal cell) and axonal projection targets. The position of the eighth retinula cell in relation to the position of the cone cell projections (Chua et al., 2023) provides a means for the unique recognition and labelling of all other cells. The accuracy of identification of the three inner and six outer PRs was proved by projections of PR axons into lamina and medulla. Position and neuronal morphology data in *Megaphragma* lead to the conclusion that the extra inner PR represents also an R7' cell, nestled between the outer PR duet R3 & R4 and facing R7 along the medial axis of the ommatidium, as noted in Friedrich et al., 2011.

Data availability

The vEM dataset generated and analyzed during the current study are available on https://waspem-lamina.flatironinstitute.org/.

The raw data of measurements available in Suppl. 2.

Acknowledgement

This work was supported by the Russian Science Foundation (project no. 22-14-00028, A.A.P.).

Author contributions

Conceptualization: ideas; formulation of the overarching research goals and aims (A.A.M., A.A.P.)

Methodology: development or design of methodology or creation of models (A.A.M., N.J.C., P.G., S.P., C.S.X., H.F.H, A.A.P.)
Formal analysis: application of statistical, mathematical, computational, or other techniques to analyze or summarize data (A.A.M., N.J.C., A.A.P.)
Writing—original draft: preparation, creation and/or presentation of the published work, specifically writing the initial draft (A.A.M.)
Writing—review and editing: critical review, commentary, or revision (A.A.M., N.J.C., A.V.D., I.A.D., S.P., C.S.X., H.F.H., D.B.C., A.A.P.)
Visualization: preparation, creation and/or presentation of the published work, specifically data presentation or visualization (A.A.M.)
Supervision: oversight and leadership responsibilities, including mentorship (A.A.M., H.F.H., D.B.C., A.A.P)
Funding acquisition: acquisition of financial support (A.A.P.)

References

Aepli, F., Labhart, T., & Meyer, E. P. (1985). Structural specializations of the cornea and retina at the dorsal rim of the compound eye in hymenopteran insects. Cell and Tissue Research, 239(1), 19–24. https://doi.org/10.1007/BF00214897

Awata, H., Matsushita, A., Wakakuwa, M., & Arikawa, K. (2010). Eyes with basic dorsal and specific ventral regions in the glacial Apollo, *Parnassius glacialis* (Papilionidae). The Journal of Experimental Biology, 213(Pt 23), 4023–4029. https://doi.org/10.1242/jeb.048678

Bernardo, U., & Viggiani, G. (2002). Biological data on *Megaphragma amalphitanum* Viggiani and *Megaphragma mymaripenne* Timberlake (Hymenoptera: Trichogrammatidae), egg-parasitoid of *H. haemorrhoidalis* (Bouché) (Thysanoptera: Thripidae) in southern Italy. Bollettino Del Laboratorio Di Entomologia Agraria "Filippo Silvestri," 58, 77–85.

Błaszczak, Z., Kreysing, M., & Guck, J. (2014). Direct observation of light focusing by single photoreceptor cell nuclei. Optics Express, 22(9), 11043. https://doi.org/10.1364/oe.22.011043

Borst, A. (2009). *Drosophila's* View on Insect Vision. Current Biology, 19 (1), R36-R47. https://doi.org/10.1016/j.cub.2008.11.001

Borst, A., Egelhaaf, M. (1989). Principles of visual motion detection. TINS, 12 (8), 297-306. https://doi.org/10.1016/0166-2236(89)90010-6

Chua, N. J., Makarova, A. A., Gunn, P., Villani, S., Cohen, B., Thasin, M., Wu, J., Shefter, D., Pang, S., Xu, C. S., Hess, H. F., Polilov, A. A., & Chklovskii, D. B. (2023). A complete reconstruction of the early visual system of an adult insect. Current Biology, 33(21), 4611-4623.e4. https://doi.org/10.1016/j.cub.2023.09.021

Cook, S. J., Jarrell, T. A., Brittin, C. A., Wang, Y., Bloniarz, A. E., Yakovlev, M. A., Nguyen, K. C. Q., Tang, L. T. H., Bayer, E. A., Duerr, J. S., Bülow, H. E., Hobert, O., Hall, D. H., & Emmons, S. W. (2019). Whole-animal connectomes of both *Caenorhabditis elegans* sexes. Nature, 571, 63–71. https://doi.org/10.1038/s41586-019-1352-7

Desyatirkina, I. A., Makarova, A. A., Pang, S., Xu, C. S., Hess, H., & Polilov, A. A. (2023). Multiscale head anatomy of *Megaphragma* (Hymenoptera: Trichogrammatidae). Arthropod Structure and Development, 76, 101299. https://doi.org/10.1016/j.asd.2023.101299

Diakova, A. V., Makarova, A. A., Pang, S., Xu, C. S., Hess, H., & Polilov, A. A. (2022). The 3D ultrastructure of the chordotonal organs in the antenna of a microwasp remains complex although simplified. Scientific Reports, 12(1), 1–13. https://doi.org/10.1038/s41598-022-24390-4

Fischer, S., Lu, Z., & Meinertzhagen, I. A. (2018). From two to three dimensions: The importance of the third dimension for evaluating the limits to neuronal miniaturization in insects. Journal of Comparative Neurology, 526(4), 653–662. https://doi.org/10.1002/cne.24358

Fischer, S., Lu, Z., & Meinertzhagen, I. A. (2019). Three-dimensional ultrastructural organization of the ommatidium of the minute parasitoid wasp *Trichogramma evanescens*. Arthropod Structure and Development, 48, 35–48. https://doi.org/10.1016/j.asd.2018.12.003

Fischer, S., Meyer-Rochow, V. B., & Müller, C. H. G. (2012). Challenging limits: Ultrastructure and size-related functional constraints of the compound eye of *Stigmella microtheriella* (Lepidoptera: Nepticulidae). Journal of Morphology, 273(9), 1064–1078. https://doi.org/10.1002/jmor.20045

Fischer, S., Meyer-Rochow, V. B., & Müller, C. H. G. (2014). Compound eye miniaturization in Lepidoptera: A comparative morphological analysis. Acta Zoologica, 95, 438–464. https://doi.org/10.1111/azo.12041

Fischer, S., Müller, C. H. G., & Meyer-Rochow, V. B. (2010). How small can small be: The compound eye of the parasitoid wasp *Trichogramma evanescens* (Westwood, 1833) (Hymenoptera, Hexapoda), an insect of 0.3- to 0.4-mm total body size. Visual Neuroscience, 28(4), 295–308. https://doi.org/10.1017/S0952523810000192

Fischer, S., Müller, C. H. G., & Meyer-Rochow, V. B. (2011). Neither apposition nor superposition: The compound eyes of the Chestnut Leafminer *Cameraria ohridella*. Zoomorphology, 131(1), 37–55. https://doi.org/10.1007/s00435-011-0141-0

Friedrich, M., Wood, E. J., & Wu, M. (2011). Developmental evolution of the insect retina: Insights from standardized numbering of homologous photoreceptors. Journal of Experimental Zoology Part B: Molecular and Developmental Evolution, 316 B(7), 484–499. https://doi.org/10.1002/jez.b.21424

Graham, P., Philippides, A. (2012). Insect-Inspired Vision and Visually Guided Behavior. In: Bhushan, B. (eds) Encyclopedia of Nanotechnology. Springer, Dordrecht. https://doi.org/10.1007/978-90-481-9751-4_221

Greiner, B., Cronin, T. W., Ribi, W. A., Wcislo, W. T., & Warrant, E. J. (2007). Anatomical and physiological evidence for polarisation vision in the nocturnal bee *Megalopta genalis*. Journal of Comparative Physiology A: Neuroethology, Sensory, Neural, and Behavioral Physiology, 193, 591–600. https://doi.org/10.1007/s00359-007-0214-1

Greiner, B., Ribi, W. A., & Warrant, E. J. (2004). Retinal and optical adaptations for nocturnal vision in the halictid bee *Megalopta genalis*. Cell and Tissue Research, 316, 377–390. https://doi.org/10.1007/s00441-004-0883-9

Gribakin, F. G. (1972). The distribution of the long wave photoreceptors in the compound eye of the honey bee as revealed by selective osmic staining. Vision Research, 12(7). https://doi.org/10.1016/0042-6989(72)90193-9

Gribakin, F. G. (1975). Functional morphology of the compound eye of the bee. In G. A. Horridge (Ed.), The Compound Eye and Vision of Insects (pp. 154–175). Oxford University Press.

Gribakin, F.G. (1981). Mechanisms of photoreception in insects (214 p.) Nauka (In Russian).

Gutiérrez, D., Rigosi, E., Nagloo, N., O'Carroll, D., Warrant, E.J. (2024). Spatial resolution and optical sensitivity in the compound eyes of two common European wasps, *Vespula germanica* and *Vespula vulgaris.* Journal of Experimental Biology, 227, jeb246670. doi:10.1242/jeb.246670

Herrling, P. L. (1976). Regional distribution of three ultrastructural retinula types in the retina of *Cataglyphis bicolor* Fabr. (Formicidae, Hymenoptera). Cell and Tissue Research, 169(2), 247–266. https://doi.org/10.1007/BF00214212

Honkanen, A., & Meyer-Rochow, V. B. (2009). The eye of the parthenogenetic and minute moth *Ectoedemia argyropeza* (Lepidoptera: Nepticulidae). European Journal of Entomology, 106, 619–629. https://doi.org/10.14411/eje.2009.078

Jékely, G., Jasek, S., Gühmann, M., Bezares-Calderón, L. A., Williams, E. A., & Shahidi, R. (2024). Whole-body connectome of a segmented annelid larva. BioRxiv, 1, 2024.03.17.585258. http://biorxiv.org/content/early/2024/03/17/2024.03.17.585258.abstract

Kawasaki, Y., Matsumoto, A., Miyaki, T., Kinoshita, M., Kakuta, S., Sakai, T., & Ichimura, K. (2019). Three-dimensional architecture of pericardial nephrocytes in *Drosophila melanogaster* revealed by FIB/SEM tomography. Cell and Tissue Research, 378(2), 289–300. https://doi.org/10.1007/s00441-019-03037-3

Labhart, T. (1980). Specialized photoreceptors at the dorsal rim of the honeybee's compound eye: Polarizational and angular sensitivity. Journal of Comparative Physiology A, 141(1), 19–30. https://doi.org/10.1007/BF00611874

Labhart, T., Baumann, F., & Bernard, G. D. (2009). Specialized ommatidia of the polarization-sensitive dorsal rim area in the eye of monarch butterflies have non-functional reflecting tapeta. Cell and Tissue Research, 338(3), 391–400. https://doi.org/10.1007/s00441-009-0886-7

Labhart, T., & Meyer, E. P. (1999). Detectors for polarized skylight in insects: A survey of ommatidial specializations in the dorsal rim area of the compound eye. Microscopy Research and Technique, 47(6), 368–379. https://doi.org/10.1002/(SICI)1097-0029(19991215)47:6<368::AID-JEMT2>3.0.CO;2-Q

Makarova, A. A., Diakova, A. A., Chaika, S. Y., & Polilov, A. A. (2022a). Scaling of the Sense Organs of Insects. 1. Introduction. Compound Eyes. Entomological Review, 102(2), 161–181. https://doi.org/10.1134/S0013873822020026

Makarova, A. A., Diakova, A. A., Chaika, S. Y., & Polilov, A. A. (2022b). Scaling of the Sense Organs of Insects. 2. Sensilla. Discussion. Conclusion. Entomological Review, 102(3), 323–346. https://doi.org/10.1134/S0013873822030058

Makarova, A. A., Meyer-Rochow, V. B., & Polilov, A. A. (2019). Morphology and scaling of compound eyes in the smallest beetles (Coleoptera: Ptiliidae). Arthropod Structure and Development, 48, 83–97. https://doi.org/10.1016/j.asd.2019.01.001

Makarova, A. A., & Polilov, A. A. (2018). Structure and Ultrastructure of the *Acrotrichis grandicollis* (Coleoptera: Ptiliidae) Compound Eyes and the Eye Features Related to Miniaturisation. Doklady Biological Sciences, 480(1), 97–99. https://doi.org/10.1134/S0012496618030067

Makarova, A. A., Veko, E. N., & Polilov, A. A. (2022). Metamorphosis and denucleation of the brain in the miniature wasp *Megaphragma viggianii* (Hymenoptera: Trichogrammatidae). Arthropod Structure and Development, 70, 101200. https://doi.org/10.1016/j.asd.2022.101200

Makarova, A., Polilov, A., & Fischer, S. (2015). Comparative morphological analysis of compound eye miniaturization in minute hymenoptera. Arthropod Structure and Development, 44(1), 21–32. https://doi.org/10.1016/j.asd.2014.11.001

Matsushita, A., Awata, H., Wakakuwa, M., Takemura, S. ya, & Arikawa, K. (2012). Rhabdom evolution in butterflies: Insights from the uniquely tiered and heterogeneous ommatidia of the Glacial Apollo butterfly, *Parnassius glacialis*. Proceedings of the Royal Society B: Biological Sciences, 279(1742), 3482–3490. https://doi.org/10.1098/rspb.2012.0475

Meinertzhagen, I. A. (2018). Of what use is connectomics? A personal perspective on the Drosophila connectome. Journal of Experimental Biology, 221(10). https://doi.org/10.1242/jeb.164954

Meinertzhagen, I. A., Menzel, R., & Kahle, G. (1983). The identification of spectral receptor types in the retina and lamina of the dragonfly *Sympetrum rubicundulum*. Journal of Comparative Physiology □ A, 151(3), 295–310. https://doi.org/10.1007/BF00623906

Menzel, J. G., Wunderer, H., & Stavenga, D. G. (1991). Functional morphology of the divided compound eye of the honeybee drone (*Apis mellifera*). Tissue and Cell, 23(4), 525–535. https://doi.org/10.1016/0040-8166(91)90010-Q

Menzel, R., & Snyder, A. W. (1974). Polarised light detection in the bee, *Apis mellifera*. Journal of Comparative Physiology, 88(3), 247–270. https://doi.org/10.1007/BF00697958

Meyer-Rochow, V.B., (2015). Compound eyes of insects and crustaceans: some examples that show there is still a lot of work left to be done. Insect Sci. 22, 461e481.

Meyer-Rochow, V. B., & Gál, J. (2004). Dimensional limits for arthropod eyes with superposition optics. Vision Research, 44(19), 2213–2223. https://doi.org/10.1016/j.visres.2004.04.009

Meyer-Rochow, V. B., & Yamahama, Y. (2019). Consequences of extreme miniaturization: The ultrastructure of the compound eyes of a 0.65 mm long “three-eyed” gall midge (Diptera; Cecidomyiidae). Entomologie Beute, 31, 1–15.

Mohr, T., & Fischer, S. (2020). Ultrastructural evidence for the origin of the subretinal pigment shield in the compound eye of Drosophila melanogaster. Journal of Morphology, 281(7), 802–807. https://doi.org/10.1002/jmor.21143

Narendra, A., Alkaladi, A., Raderschall, C. A., Robson, S. K. A., & Ribi, W. A. (2013). Compound eye adaptations for diurnal and nocturnal lifestyle in the intertidal ant, *Polyrhachis sokolova*. PLoS ONE, 8(10), e76015. https://doi.org/10.1371/journal.pone.0076015

Nilsson, D. E., Labhart, T., & Meyer, E. (1987). Photoreceptor design and optical properties affecting polarization sensitivity in ants and crickets. Journal of Comparative Physiology A, 161(5), 645–658. https://doi.org/10.1007/BF00605006

Palavalli-Nettimi, R., & Narendra, A. (2018). Miniaturisation decreases visual navigational competence in ants. The Journal of Experimental Biology, 221(7), jeb177238. https://doi.org/10.1242/jeb.177238

Palavalli-Nettimi, R., Ogawa, Y., Ryan, L. A., Hart, N. S., & Narendra, A. (2019). Miniaturisation reduces contrast sensitivity and spatial resolving power in ants. Journal of Experimental Biology, 222, jeb203018. https://doi.org/10.1242/jeb.203018

Plaza, S. M., Scheffer, L. K., & Chklovskii, D. B. (2014). Toward large-scale connectome reconstructions. Current Opinion in Neurobiology, 25, 201–210. https://doi.org/10.1016/j.conb.2014.01.019

Polaszek, A., Fusu, L., Viggiani, G., Hall, A., Hanson, P., & Polilov, A. A. (2022). Revision of the World Species of *Megaphragma* Timberlake (Hymenoptera: Trichogrammatidae)†. Insects, 13(6), 1–66. https://doi.org/10.3390/insects13060561

Polilov, A. A. (2012). The smallest insects evolve anucleate neurons. Arthropod Structure and Development, 41(1), 29–34. https://doi.org/10.1016/j.asd.2011.09.001

Polilov, A. A. (2017). Anatomy of adult Megaphragma (Hymenoptera: Trichogrammatidae), one of the smallest insects, and new insight into insect miniaturization. PLoS ONE, 12(5), e0175566. https://doi.org/10.1371/journal.pone.0175566

Polilov, A. A., Makarova, A. A., Pang, S., Shan Xu, C., & Hess, H. (2021). Protocol for preparation of heterogeneous biological samples for 3D electron microscopy: a case study for insects. Scientific Reports, 11, 4717. https://doi.org/10.1038/s41598-021-83936-0

Ribi, W. A. (1975). The first optic ganglion of the bee. I. Correlation between visual cell types and their terminals in the lamina and medulla. Cell and Tissue Research, 165, 103–111. https://doi.org/10.1007/bf00234847

Ryan, K., Lu, Z., & Meinertzhagen, I. A. (2016). The CNS connectome of a tadpole larva of *Ciona intestinalis* (L.) highlights sidedness in the brain of a chordate sibling. ELife, 5, e16962. https://doi.org/10.7554/eLife.16962

Schinz, R. H. (1975). Structural Specialization in the Dorsal Retina of the Bee, *Apis mellifera*. Cell and Tissue Research, 34, 23–34. https://doi.org/10.1007/BF00223259

Schmitt, M., Mischke, U., & Wachmann, E. (1982). Phylogenetic and Functional Implications of the Rhabdom Patterns in the Eyes of Chrysomeloidea (Coleoptera). Zoologica Scripta, 11(1), 31–44. https://doi.org/10.1111/j.1463-6409.1982.tb00516.x

Serres, J. R., Viollet, S. (2018). Insect-inspired vision for autonomous vehicles. Current Opinion in Insect Science, 30, 46-51. https://doi.org/10.1016/j.cois.2018.09.005

Sharko, F. S., Nedoluzhko, A. V., Lê, B. M., Tsygankova, S. V., Boulygina, E. S., Rastorguev, S. M., Sokolov, A. S., Rodriguez, F., Mazur, A. M., Polilov, A. A., Benton, R., Evgen'ev, M. B., Arkhipova, I. R., Prokhortchouk, E. B., & Skryabin, K. G. (2019). A partial genome assembly of the miniature

parasitoid wasp, *Megaphragma amalphitanum*. PLoS ONE, 14(12), e0226485. https://doi.org/10.1371/journal.pone.0226485

Solovei, I., Kreysing, M., Lanctôt, C., Kösem, S., Peichl, L., Cremer, T., Guck, J., & Joffe, B. (2009). Nuclear Architecture of Rod Photoreceptor Cells Adapts to Vision in Mammalian Evolution. Cell, 137(2), 356–368. https://doi.org/10.1016/j.cell.2009.01.052

Spaethe, J., & Briscoe, A. D. (2005). Molecular characterization and expression of the UV opsin in bumblebees: Three ommatidial subtypes in the retina and a new photoreceptor organ in the lamina. Journal of Experimental Biology, 208(12), 2347–2361. https://doi.org/10.1242/jeb.01634

Srinivasan, M.V., Chahl, J.S., Weber, K., Venkatesh, S., Nagle, M.G., Zhang, S.W. (1999). Robot navigation inspired by principles of insect vision. Robotics and Autonomous Systems, 26(2–3), 203-216. https://doi.org/10.1016/S0921-8890(98)00069-4

Stavenga, D. G. (2002). Colour in the eyes of insects. Journal of Comparative Physiology A: Neuroethology, Sensory, Neural, and Behavioral Physiology, 188(5), 337–348. https://doi.org/10.1007/s00359-002-0307-9

Stavenga, D. G., & Hardie, R. C. (Eds.). (1989). Facets of Vision. Springer-Verlag. https://doi.org/10.1017/CBO9781107415324.004

Strausfeld, N.J. (1989). Insect Vision and Olfaction: Common Design Principles of Neuronal Organization. In: Singh, R.N., Strausfeld, N.J. (eds) Neurobiology of Sensory Systems. Springer, Boston, MA. https://doi.org/10.1007/978-1-4899-2519-0_2

Takemura, S. Y., & Arikawa, K. (2006). Ommatidial type-specific interphotoreceptor connections in the lamina of the swallowtail butterfly, *Papilio xuthus*. Journal of Comparative Neurology, 494(4), 663–672. https://doi.org/10.1002/cne.20830

Tomlinson, A. (2012). The origin of the *Drosophila* subretinal pigment layer. Journal of Comparative Neurology, 520(12), 2676–2682. https://doi.org/10.1002/cne.23063

Varshney, L. R., Chen, B. L., Paniagua, E., Hall, D. H., & Chklovskii, D. B. (2011). Structural properties of the *Caenorhabditis elegans* neuronal network. PLoS Computational Biology, 7(2), e1001066. https://doi.org/10.1371/journal.pcbi.1001066

Wakakuwa, M., Stavenga, D. G., & Arikawa, K. (2007). Spectral Organization of Ommatidia in Flower-visiting Insects†. Photochemistry and Photobiology, 83(1), 27–34. https://doi.org/10.1562/2006-03-03-ir-831

Warrant, E. J., McIntyre, P.D. (1993). Arthropod eye design and the physical limits to spatial resolving power. Progress in Neurobiology, 40(4), 413-461. https://doi.org/10.1016/0301-0082(93)90017-M

Warrant, E., Nilsson, D.-E. (Eds.) (2006). Invertebrate Vision. Cambridge University Press.

White, J. G., Southgate, E., Thomson, J. N., & Brenner, S. (1986). The Structure of the Nervous System of the Nematode *Caenorhabditis elegans*. Philosophical Transactions of the Royal Society B: Biological Sciences, 314(1165), 1–340. https://doi.org/10.1098/rstb.1986.0056

Wolff, T., & Ready, D. F. (1991). Cell death in normal and rough eye mutants of *Drosophila.* Development, 113(3), 825–839. https://doi.org/10.1242/dev.113.3.825

Xu, C. S., Hayworth, K. J., Lu, Z., Grob, P., Hassan, A. M., García-Cerdán, J. G., Niyogi, K. K., Nogales, E., Weinberg, R. J., & Hess, H. F. (2017). Enhanced FIB-SEM systems for large-volume 3D imaging. ELife, 6, 1–36. https://doi.org/10.7554/eLife.25916

Xu, C. S., Pang, S., Shtengel, G., Müller, A., Ritter, A. T., Hoffman, H. K., Takemura, S. ya, Lu, Z., Pasolli, H. A., Iyer, N., Chung, J., Bennett, D., Weigel, A. V., Freeman, M., van Engelenburg, S. B., Walther, T. C., Farese, R. V., Lippincott-Schwartz, J., Mellman, I., … Hess, H. F. (2021). An open-access volume electron microscopy atlas of whole cells and tissues. Nature, 599(7883), 147–151. https://doi.org/10.1038/s41586-021-03992-4

Supplement 1

EM cross-sections of the *M. viggianii* ommatidia.

Supplement 2

The raw data for all measurements of ommatidia.

Table S1. Linear measurements of ommatidia in *M. viggianii*.

Table S2. Volumetric measurements for cellular and subcellular elements of all 29 ommatidia in *M. viggianii*.

Table S3. The percentage of cell occupied by organelles.

Table S4. Optical properties of the compound eye of *M. viggianii*.

Supplement 3

Video 1. 3D reconstruction of the ultrastructure of the compound eye of *M. viggianii*

Video 2. 3D reconstruction of the ultrastructure of the DRA and Reg ommatidia in *M. viggianii*.

Impact statement:

Even the smallest compound eyes retain the functional specialization of ommatidia